BOREAS An international journal of Quaternary research

Late-Holocene evolution of a small Sub-Arctic glacier, Gljúfurárjökull (Tröllaskagi, northern Iceland)

NURIA ANDRÉS, JOSÉ M. FERNÁNDEZ-FERNÁNDEZ, DAVID PALACIOS, IRENE SCHIMMELPFENNIG, LEOPOLDO G. SANCHO, SKAFTI BRYNJÓLFSSON, ÞORSTEINN SÆMUNDSSON, WESLEY R. FARNSWORTH, LUIS M. TANARRO, MARIANO BRITO, JAVIER SANTOS-GONZÁLEZ, ROSA B. GONZÁLEZ-GUTIÉRREZ, ASTER TEAM, GEORGES AUMAÎTRE AND KARIM KEDDADOUCHE

BOREAS

Andrés, N., Fernández-Fernández, J. M., Palacios, D., Schimmelpfennig, I., Sancho, L. G., Brynjólfsson, S., Sæmundsson, Þ., Farnsworth, W. R., Tanarro, L. M., Brito, M., Santos-González, J., González-Gutiérrez, R. B. & ASTER Team: Late-Holocene evolution of a small Sub-Arctic glacier, Gljúfurárjökull (Tröllaskagi, northern Iceland). *Boreas*. https://doi.org/10.1111/bor.70030. ISSN 0300-9483.

Gljúfurárjökull, located on the Tröllaskagi Peninsula in northern Iceland, is a small glacier approximately 3.8 km in length. This study analyses the glacier's evolution through a combination of methods including: (i) geomorphological mapping, (ii) Cosmic-Ray Exposure (CRE) dating, (iii) lichenometry and (iv) palaeoglacier reconstruction (volume, extent and Equilibrium Line Altitude (ELA)) for each identified ice-marginal position. The mean CRE ages obtained are as follows: Glacial Phase 1: no samples available for CRE dating; Glacial Phase 2: 2.6±0.5 ka ($n = 2$); Glacial Phase 3: 3.2±1.1 ka (n = 7); Glacial Phase 4: 2.5±0.2 ka ($n = 2$); Glacial Phase 5: between 2.1 ka and a few hundred years. Lichenometry results for surfaces older than 130 years show inconsistencies both internally and in comparison with CRE ages. However, for the most recent glacier margins, lichenometric dates are coherent and align with historical photographic evidence. Accordingly, the ages proposed for glacier marginal positions 6 and 7 are 1899/1904 CE and 1912/1917 CE, respectively, slightly predating position 8, which is documented in aerial photographs from 1946 CE. The millennial- to centennial-scale evolution of Gljúfurárjökull outlined in this study is consistent with the patterns observed in debris-free glaciers across Tröllaskagi, as well as in many Icelandic and Arctic glaciers. Notably, the Little Ice Age (LIA) advance at Gljúfurárjökull was less extensive than earlier Neoglacial advances, a trend common in the Sub-Arctic and Arctic regions. Since the end of the LIA, the glacier has experienced a general retreat, interrupted only by a brief advance during the 1980s–1990s—again mirroring broader Arctic glacial behaviour. Overall, this study underscores the high sensitivity of Gljúfurárjökull to climatic fluctuations during the Late Holocene. The application of CRE dating reveals that the glacier's evolution aligns closely with patterns observed in other Icelandic and Arctic glaciers.

Nuria Andrés (nandresp@ucm.es), José M. Fernández-Fernández, David Palacios, Luis M. Tanarro and Mariano Brito, Department of Geography, Universidad Complutense de Madrid, 28040 Madrid, Spain; Irene Schimmelpfennig and ASTER Team (Consortium: Georges Aumaître, Karim Keddadouche), Aix-Marseille Université, CNRS, IRD, INRAE, Coll. France, UM 34 CEREGE, Technopôle de l'Environnement Arbois-Méditerranée, BP 80, 13545 Aix-en-Provence, France; Leopoldo G. Sancho, Department of Pharmacology, Pharmacognosy and Botany, Universidad Complutense de Madrid, 28040 Madrid, Spain; Skafti Brynjólfsson, Icelandic Institute of Natural History, 600 Akureyri, Iceland; Þorsteinn Sæmundsson, Institute of Earth Sciences, University of Iceland, 102 Reykjavík, Iceland; Wesley R. Farnsworth, Institute of Earth Sciences, University of Iceland, 102 Reykjavík, Iceland and Globe Institute, University of Copenhagen, 1350 Copenhagen, Denmark; Javier Santos-González and Rosa B. González-Gutiérrez Department of Geography and Geology, Universidad de León, 24004 León, Spain; *received 6th December 2024, accepted 15th July 2025.*

The debris-free glacier Gljúfurárjökull (65°43′N, 18°39′W; Fig. 1), located in the Tröllaskagi Peninsula, has attracted scientific interest since the early 20th century. Icelandic researchers began observing its evolution as early as the 1930s (Eyþórsson 1963; Rist 1974), and its extent has been monitored continuously from the late 19th century to the present day (Icelandic Glacier Web Portal, https://islenskirjoklar.is). Since 1977, special attention has been devoted not only to monitoring the glacier but also to reconstructing its past evolution. The first step in this effort was the mapping of a complex series of moraines located beyond the current glacier margin (Caseldine & Cullingford 1981). Using vegetation cover and diversity, the formation age of each end moraine was estimated. These studies concluded that the outermost moraine likely formed during the final phase of the Little Ice Age (LIA), around the end of the 19th century (Caseldine & Cullingford 1981). Subsequent work applied lichenometry (*Rhizocarpon geographicum*) to more accurately determine moraine ages in the Gljúfurárdalur valley. Growth rates of 0.57 mm a^{-1} (for the single largest lichen) and 0.51 mm a^{-1} (mean of the five largest lichens) were used, confirming that the glacier reached its Late Holocene maximum advance between 1898 and 1903 CE (Caseldine 1983).

The evolution of Gljúfurárjökull proposed in these early studies seems to align with broader syntheses by Hannesdóttir *et al.* (2020) and AÞalgeirsdóttir *et al.* (2020), which suggest that most Icelandic glaciers reached their maximum extent during the Late Holocene (4.2 ka to present), particularly at the end of the 19th century. However, some glaciers may have reached their maximum extent earlier, during the 18th century. The culmination of the LIA is considered the greatest ice

DOI 10.1111/bor.70030

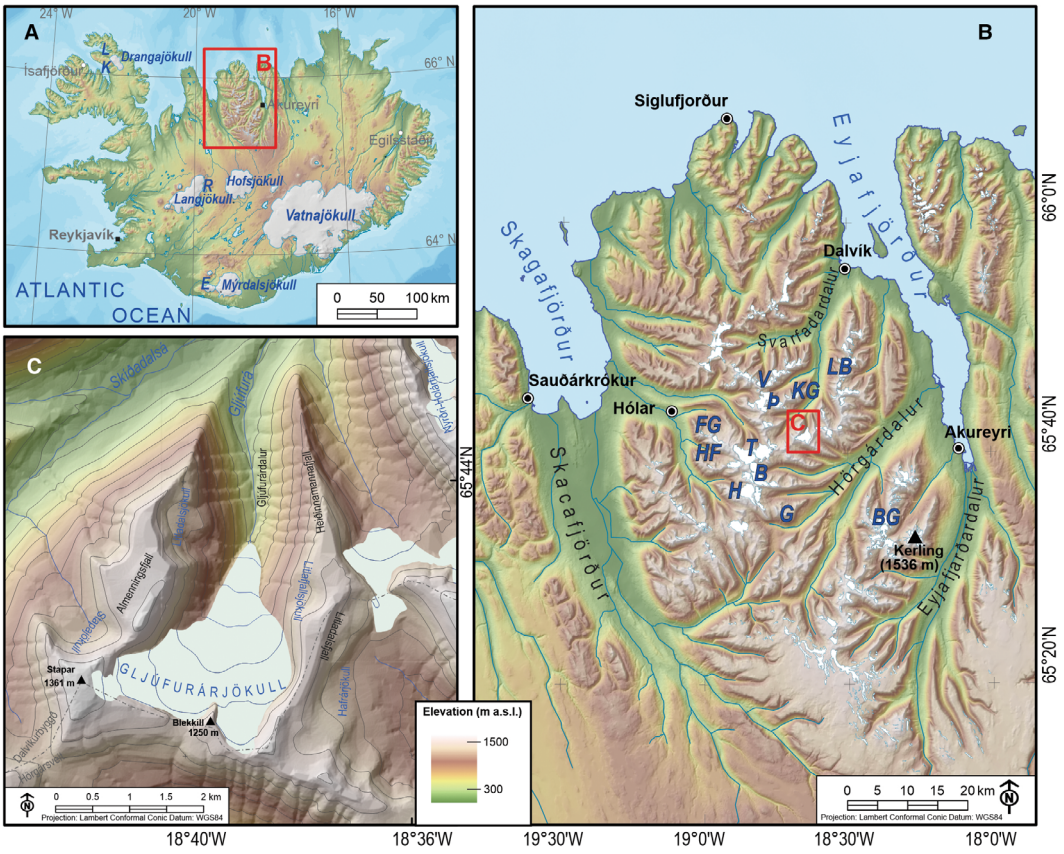

Fig. 1. Location of the Gljúfurárjökull in the Tröllaskagi Peninsula. A. Iceland. Tröllaskagi map and glaciers cited in the text. L = LeirufjörÞur; K = Kaldalón Valley; R = RegnbúÞajökull ice cap; E = Eyjafjallajökull; The red box delimits the Trollaskagui peninsula. B. Map of the Trollaskagui peninsula; BG = Bægisárdalur; B = Barkárdalur; V = Vatnsdalur; G = Grænavatn; LB = Lambárdalur; KG = KóngsstaÞadalur; Þ = Þverárdalur; T = Tungnahryggsjökull; The red box delimits the study area. C. Study area of Gljúfurárjökull.

extent since the Preboreal oscillation (11.3–10.7 ka BP; Fisher *et al.* 2002). Preboreal advances were significantly larger than those during the Late Holocene, with associated landforms and deposits often hundreds of meters beyond LIA features (Hannesdóttir *et al.* 2020).

Nonetheless, to these affirmations, some Late Holocene (Neoglacial) moraines pre-dating the LIA are located just a few meters beyond the LIA maximum and behind the older Preboreal moraines (Hannesdóttir *et al.* 2020; Benediktsson *et al.* 2024), as previously suggested by Eyþórsson (1935) and Thorarinsson (1946, 1949). In fact, the extent of Icelandic glaciers during different periods of the Holocene remains a topic of active research and debate (Benediktsson *et al.* 2024). Dugmore (1989) and Dugmore & Sugden (1991) used tephrochronology to show that maximum glacier extents in southern Iceland occurred prior to 3.1 ka. Gudmundsson (1997) synthesized moraine chronologies outside the LIA limits, identifying glacial advances at ~5–4.5, 4.2, 3, 2, 1.5–1.2 cal. ka BP and during the LIA. Later, Kirkbride and Dugmore (2006) dated aeolian soils associated with moraine ridges in RegnbúÞajökull (central Iceland), identifying advances at 4.5–5.0, 3.0–3.5, ~2.0–2.5 cal. ka BP and during the LIA (~1700 CE and late 19th century). Using a combination of tephrochronology and lichenometry, Kirkbride & Dugmore (2008) documented glacier advances in Eyjafjallajökull (southern Iceland) before the 3rd century, during the 9th and 12th centuries, and five more between 1700 and 1930 CE. In NW Iceland, Principato (2008) radiocarbon dated wood from a Kaldalón Valley moraine (SE Drangajökull), yielding an age of 2.5 cal. ka BP and highlighting pre-LIA glacial activity.

These findings—of more extensive glacial advances during early Neoglacial phases than during the LIA—raise questions about the reliability of lichenometry for dating older moraines, including those at Gljúfurárjökull. Indeed, lichenometry was also applied by Caseldine (1985) to Tungnahryggsjökull moraines, estimating an outermost moraine age of 1876–1878 CE. However, cosmic-ray exposure (CRE) dating on the same moraine yielded an age of 1480±100 CE (Fernández-Fernández *et al.* 2019). In Vesturdalur, the presumed LIA maximum moraine (previously assigned to the 19th century; Caseldine 1985; Caseldine & Stötter 1993; Hannesdóttir *et al.* 2020)

could not be dated due to erosion. Nonetheless, CRE exposure ages on other moraines revealed pre-LIA advances at ~400 and ~700 CE (corresponding to the Dark Ages Cold Period; Helama *et al.* 2017), and several LIA advances from the 15th to 17th centuries.

The divergence between results from lichenometry and CRE dating in Tungnahryggsjökull underscores concerns about the validity of lichenometry for dating older than ~200 years, a limitation acknowledged by earlier researchers. In later syntheses, a constant growth rate of 0.44 mm a^{-1} and a 10-year colonization lag were assumed for *Rhizocarpon geographicum* (Häberle 1991; Kugelmann 1991). These parameters yielded five main glacial expansion periods in Tröllaskagi: 1810–1820 CE, 1845–1875 CE, late 1880s–early 1890s CE, 1915–1925 CE and late 1930s–early 1940s CE. However, outermost moraines (pre-1800) remain undated by this method. Combined with evidence of significant cooling from 5.8 cal. ka BP, this suggests the potential for major glacial advances during the late Middle Holocene (Caseldine & Hatton 1994).

Holocene glacier advances in Tröllaskagi have long been debated. While many researchers agree that maximum post-Preboreal glacial extent was reached during the late 19th century (Caseldine & Stötter 1993; Hannesdóttir *et al.* 2020), evidence from other dating methods suggests more extensive earlier Neoglacial advances. Häberle (1991) reported pre-LIA advances in Bægisárdalur and Barkárdalur at ~4.2, 2.2–1.8 and 1 cal. ka BP. Stötter (1991) dated moraines in Vatnsdalur to 6–4.8 and 3.4–2.8 cal. ka BP. Stötter *et al.* (1999) identified six pre-LIA advances at ~4.7, 4.2, 3.2–3.0, 2.0, 1.5 and 1.0 cal. ka BP, linked to climatic cooling. Kirkbride & Dugmore (2001) dated a major advance in Grænavatn cirque to 6–3.8 cal. ka BP, suggesting that early Neoglacial advances in Tröllaskagi were more extensive than those during the LIA. Wastl & Stötter (2005) found pre-LIA moraines slightly outside LIA limits in three glaciers—Lambárdalur (>5.1 cal. ka BP), Þverárdalur (>4.9 cal. ka BP) and KóngsstaÞadalur (>3.5 cal. ka BP). At Þverárdalur, a moraine older than 9.0 ka—likely Preboreal—was found over 100 m down-valley from Neoglacial moraines.

In recent years, push-moraine complexes have been identified in several cirques of the peninsula, especially in front of rock and debris-covered glaciers. Many of these moraines, dated using CRE, yielded ages of 10–11 ka, indicating that Preboreal advances in Tröllaskagi were more limited compared to later Holocene advances (Fernández-Fernández *et al.* 2020; Tanarro *et al.* 2021).

At present, Gljúfurárjökull appears to be the only debris-free glacier in Tröllaskagi whose maximum post-Preboreal extent occurred during the LIA, specifically in the late 19th century. However, it is important to note that only lichenometry has been used for dating moraines in this glacier, a method with limited capacity to identify older glacial advances.

Therefore, this study aims to reconstruct the Holocene evolution of this small sub-Arctic glacier and evaluate whether its development has been consistent with the general pattern observed in other Icelandic glaciers, or whether it deviates from this trend, as indicated by earlier research. The main secondary objectives are to (i) re-examine the geomorphological mapping of the complex moraine system in front of Gljúfurárjökull, using updated maps and high-resolution satellite imagery; (ii) reassess the application of lichenometry, considering the wealth of aerial and satellite imagery available, including recent datasets; (iii) apply CRE dating techniques to determine the exposure age of moraine boulders; and (iv) assess the impacts of climate variability on Gljúfurárjökull using parameters such as glacier area, volume, mass balance and Equilibrium Line Altitude (ELA) variations. The results of this study aim to resolve discrepancies between lichenometry and CRE dating previously observed in the region.

Study area

Gljúfurárjökull is a glacier situated at the head of the Gljúfurárdalur valley, a tributary of the SkíÞadalur valley, which joins SvarfaÞardalur and ultimately flows into EyjafjörÞur near the town of Dalvík, approximately 28 km from the glacier (Fig. 1). Like much of the Tröllaskagi Peninsula, Gljúfurárjökull occupies a cirque at the head of a valley carved into Miocene basalt flows interbedded with reddish sedimentary layers (Sæmundsson *et al.* 1980; Jóhannesson & Sæmundsson 1989). The valley is flanked by the Litladalsfjall ridge to the east and the Stapar peak (1361 m a.s.l.; 65°43′33″N, 18°41′51″W) to the west. The upper section of the glacier covers nearly the entire cirque wall and reaches up to the summit, resulting in minimal debris cover. In 2019, Gljúfurárjökull spanned an area of 3.09 km^2 and extended 2788 m in length, from an elevation of 1308 m a.s.l. at its headwall to 618 m a.s.l. at its terminus.

Between 1931 and 1953 CE, the glacier experienced a 46 m retreat in response to some of the warmest decades of the 20th century (Eyþórsson 1935, 1963). By 1977 CE, the glacier front had receded 95 m from its 1946 CE position (Caseldine & Cullingford 1981). However, between 1977 CE and at least 1987 CE, the glacier advanced several tens of meters, with an average advance rate of 23–26 m a^{-1} (Caseldine 1985, 1987; Glacier Web Portal: https://islenskirjoklar.is). This advancing trend was confirmed by Fernández-Fernández *et al.* (2017), who analysed historical aerial photographs (1946, 1985, 1994 and 2000 CE) and a SPOT satellite image from 2005 CE. Nevertheless, the glacier began to retreat again around 2000, and by 2005 it had lost 31% of its volume, decreasing from 0.270 km^3 to 0.191 km^3, relative to its LIA maximum extent (Fernández-Fernández *et al.* 2017).

These observations are consistent with broader glacier trends across Iceland. According to Hannesdóttir

Table 1. Sample locations, topographic shielding factor, thickness and distance from headwall.

Sample name	Sample type	Latitude (N)	Longitude (W)	Elevation (m a.s.l.)	Shielding factor	Thickness (cm)	Distance from the headwall (m)
GLJ-1	Moraine boulder	65°44′6.72″	18°38′51.36″	511	0.9415	4.5	3509
GLJ-2	Moraine boulder	65°44′5.64″	18°38′49.92″	503	0.9398	2.0	3517
GLJ-3	Moraine boulder	65°44′6.36″	18°38′48.84″	500	0.9398	3.5	3542
GLJ-4	Moraine boulder	65°44′3.48″	18°38′50.64″	526	0.9408	3.0	3442
GLJ-5	Moraine boulder	65°44′3.48″	18°38′50.64″	526	0.9408	4.0	3442
GLJ-6	Moraine boulder	65°43′58.44″	18°38′49.20″	537	0.9386	2.5	3312
GLC-1	Moraine boulder	65°43′50.16″	18°38′52.44″	581.8	0.9400	2.0	3048
GLC-2	Moraine boulder	65°43′50.52″	18°38′51.36″	577.2	0.9451	4.0	3057
GLC-5	Moraine boulder	65°43′56.28″	18°38′54.96″	577.8	0.9423	2.5	3226
GLC-6	Moraine boulder	65°43′57.36″	18°38′51.36″	556.7	0.9441	2.8	3266
GLC-7	Moraine boulder	65°44′1.32″	18°38′48.48″	516.4	0.9417	5.0	3395
GLC-8	Moraine boulder	65°44′1.68″	18°38′49.20″	516.5	0.9422	2.4	3405
GLC-9	Moraine boulder	65°44′2.40″	18°38′51.00″	523.7	0.9434	6.9	3419
GLC-10	Moraine boulder	65°44′2.76″	18°38′49.92″	520.9	0.9430	2.4	3432
GLC-11	Moraine boulder	65°44′3.12″	18°38′49.56″	518.6	0.9428	4.0	3441

et al. (2020) and AÞalgeirsdóttir *et al.* (2020), the maximum extent of Icelandic glaciers during the Late Holocene was reached around 1890 CE. From that point until 2019 CE, approximately 16±4% of the total ice volume was lost. The most intense phase of glacier mass loss occurred between 1930–31 and 1949–50, followed by a period of stability or slight advance from the mid-1960s to 1994 CE, coinciding with cooler summer temperatures and a widespread cooling of the North Atlantic (Dickson *et al.* 1975, 1988). Glacier mass loss accelerated once again between 1994–95 and 2009–10, although after 2010 it decreased considerably, approaching a near-equilibrium state. An exception to this trend was the 2018–19 period, during which Icelandic glaciers experienced one of their greatest annual losses since 1890 CE (AÞalgeirsdóttir *et al.* 2020; Hannesdóttir *et al.* 2020). This pattern mirrors glacier mass loss observed in other Arctic regions, such as Greenland, Svalbard and Norway (AÞalgeirsdóttir *et al.* 2020 and references therein).

Material and methods

Geomorphological and glacier geometry mapping

Successive fieldwork campaigns were carried out in Gljúfurárdalur during the summers of 2010, 2012, 2015 and 2018 CE, with the objective of mapping the foreland moraines using GPS and various aerial orthophotos (National Land Survey of Iceland: 1946, 1960, 1985, 1994; and a satellite image from 2000 CE). In addition, we georeferenced the foreland map originally drawn by Caseldine (1983, 1985) to locate and survey in situ the same moraines previously studied. Former positions of the glacier snout were identified, and the glacier's geometry and extent were reconstructed through visual inspection of stereoscopic image pairs and field observations.

Mapping of glacial landforms, as well as those shaped by postglacial erosive processes, was performed using a high-resolution aerial orthophoto from 2019 CE (Loftmyndir ehf). All linear glacial features (moraine ridges) were digitized; those that were prominent, continuous and well-preserved were interpreted as marking significant glacier advances or standstills—referred to as glacial phases.

In addition to geomorphological evidence, glacier fluctuations in recent decades were reconstructed based on photo interpretation of historical aerial orthophotos from 1946, 1960, 1985, 1994 and 2000 CE (National Land Survey of Iceland), 2016 CE (Maxar's Vivid basemap via ESRI's Living Atlas) and 2019 CE (Loftmyndir ehf), as well as two satellite images—one SPOT image from 2005 and a Sentinel-2 image from 2017 CE. When delineating glacier outlines, the upper ice-marginal position was assumed to remain constant unless aerial imagery indicated otherwise, as changes in that area are typically smaller than the uncertainty introduced by the photo interpreter (Koblet *et al.* 2010).

During the 2012, 2015 and 2018 CE field campaigns, mixed sediment and residual snow from avalanches were observed on the valley floor at the end of summer, along with frequent debris flows on the valley slopes.

^{36}Cl CRE dating

CRE dating was employed to determine the ages of the moraines identified in the geomorphological map. The cosmogenic nuclide ^{36}Cl was selected due to the basaltic composition of the rocks in the study area. Sampling locations for ^{36}Cl analysis are presented in Table 1 and Figs 2–5. A total of 17 samples were collected from moraine boulders during two field campaigns: 6 in 2015 and 11 in 2018 CE. These samples correspond to boulders from five distinct moraine ridges located between 800 and 1200 m in front of the glacier terminus as of

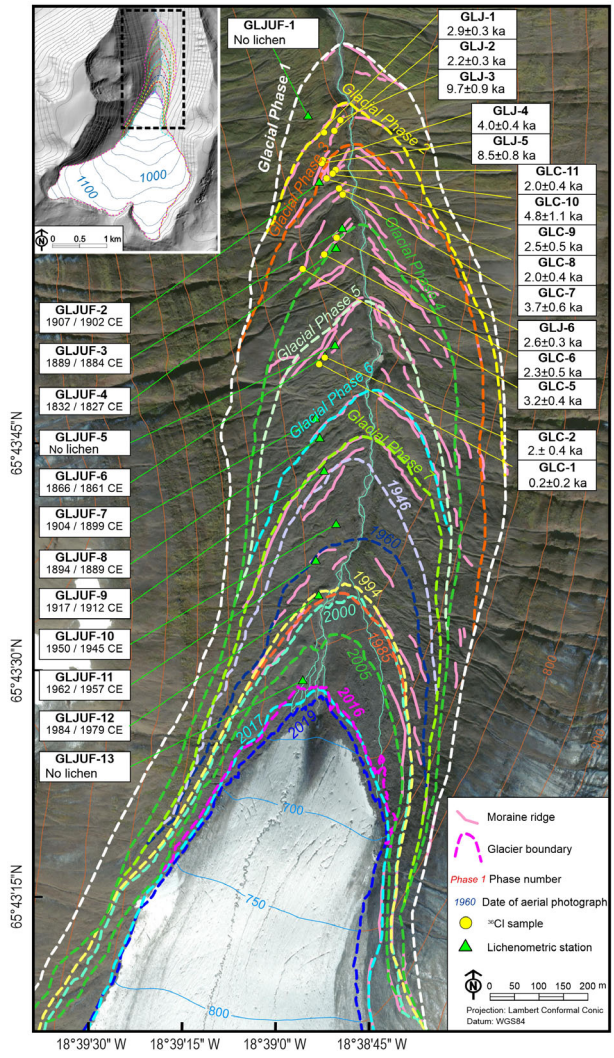

Fig. 2. Deduced glacier boundaries of the Gljúfurárjökull evolution along the Holocene according to moraine extension (phases) and historical aerial photographs and images. The location of the CRE and lichenometry results is indicated. The deduced age of each glacier boundary is also included. See justification in the text. The base orthophoto is from 2023 CE (Maxar's Vivid basemap available in the Living Atlas, ESRI).

2018 CE. The selected ridges were the best preserved and showed minimal evidence of slope-related disturbances such as debris flows or snow avalanches, which are common in the valley due to the steep (30°–40°) slopes. The outermost moraine was excluded from sampling because it was significantly affected by these processes.

Initial sample preparation was conducted at the Laboratory of Physical Geography of the Universidad Complutense de Madrid, where the rocks were crushed and sieved to obtain the 0.25–0.8 mm grain size fraction. Subsequent chemical processing was carried out at the Laboratoire National des Nucléides Cosmogéniques (LN2C) of the Centre Européen de Recherche et d'Enseignement des Géosciences de l'Environnement (CEREGE, Aix-en-Provence, France), following the procedures detailed by Schimmelpfennig *et al.* (2011). Aliquots from the bulk material of several representative samples were analysed for major and trace element compositions (Table 2), which are necessary to estimate the low-energy neutron flux in the samples.

To remove atmospheric ^{36}Cl and any Cl-rich groundmass, the samples underwent acid leaching (HNO_3 and concentrated 48% HF). From this leached material, 2-g aliquots were taken for major element analysis (Table 3). Two chemical blanks were also prepared and analysed alongside the samples (Table 4).

The final AgCl targets were measured at the AMS facility Accélérateur pour les Sciences de la Terre, Environnement et Risques (ASTER) at CEREGE. Specific isotope ratios (^{35}Cl/^{37}Cl and ^{36}Cl/^{35}Cl) were measured to determine ^{36}Cl concentrations (Table 4). These measurements were normalized using the in-house standard SM-CL-12, which has an assigned ^{36}Cl/^{35}Cl ratio of $(1.428\pm0.021)\times10^{-12}$ (Merchel *et al.* 2011), assuming a natural ^{35}Cl/^{37}Cl ratio of 3.127. Analytical uncertainties (1σ) account for AMS counting statistics and machine stability (Braucher *et al.* 2018). Due to high uncertainties in the AMS measurements for samples GLC-3 and GLC-4, these were excluded, leaving 15 valid samples for age calculation.

^{36}Cl exposure ages were calculated using the trial version of the online calculator CREp for ^{36}Cl (Martin *et al.* 2017; Schimmelpfennig *et al.* 2019; Table 2). A uniform rock density of 2.7 g cm^{-3} was assumed. Topographic shielding corrections were applied using a factor calculated with the ArcGIS toolbox developed by Li (2018), which utilizes a shapefile of sample locations and a digital elevation model (DEM) with 0.5-m resolution. This method was chosen over *in-situ* horizon measurements due to poor visibility during fieldwork.

Exposure ages were computed using the time-dependent scaling scheme of Lal/Stone (Lm) (Lal 1991; Stone 2000; Balco *et al.* 2008), incorporating the ERA40 atmospheric model (Uppala *et al.* 2005) and the LSD geomagnetic framework (Lifton *et al.* 2014). The following sea-level high-latitude (SLHL) production rates for ^{36}Cl from spallation were used: 57.3±5.2 atoms ^{36}Cl (g Ca)$^{-1}$ a^{-1} (Licciardi *et al.* 2008), 145.5±7.7 atoms ^{36}Cl (g K)$^{-1}$ a^{-1} (Schimmelpfennig *et al.* 2014), 1.628±0.04 atoms ^{36}Cl (g Fe)$^{-1}$ a^{-1} (Moore & Granger 2019) and 13±3 atoms ^{36}Cl (g Ti)$^{-1}$ a^{-1} (Fink *et al.* 2000).

Additionally, an SLHL production rate for epithermal neutrons of 691±186 neutrons (g air)$^{-1}$ a^{-1} was applied (Marrero *et al.* 2016). The resulting ^{36}Cl CRE ages and their associated analytical and total uncertainties are provided in Table 4. No corrections were applied for erosion or snow cover, in line with previous studies in Iceland (e.g. Fernández-Fernández *et al.* 2019). Notably, the sampled boulders were exposed and wind-swept, likely reducing the impact of snow accumulation.

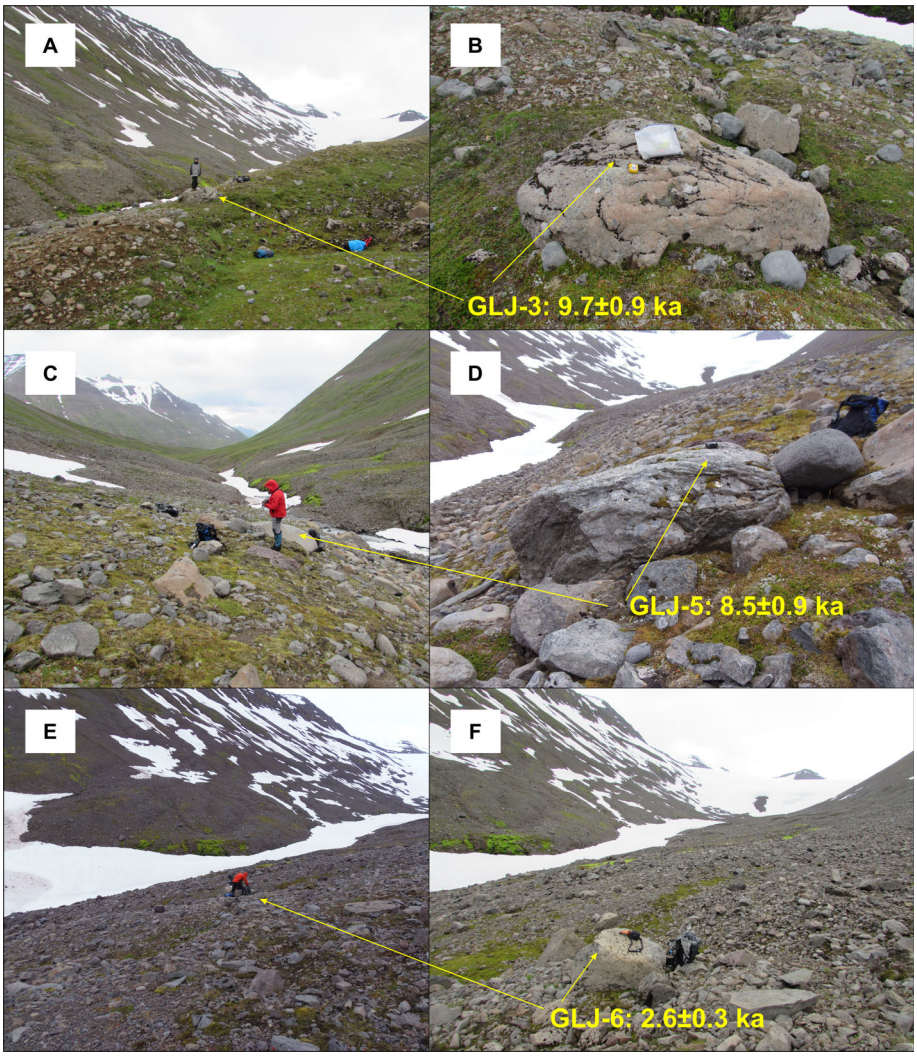

Fig. 3. Some examples of boulders sampled for CRE dating in well-preserved segments of the moraines and their results, taken in 2015 CE. A, B. Segment of one of the Phase 2 moraines, the oldest dated, with two of their oldest boulders. C, D, E, F. boulder sampled from a moraine segment of Phase 4. At the bottom of the valley, the remains of snow avalanches can be observed that last most of the summer. In photos A, D, E and F, the Gljúfurárjökull can be seen in the background. Photos of August 2015.

The dating protocol follows that described by Fernández-Fernández *et al.* (2019), ensuring full comparability between the lichenometric and CRE age results obtained in this study and those from nearby glaciers, such as Tungnahryggsjökull, which share similar characteristics and sizes.

Lichenometric dating

Lichenometry was applied to date boulders on moraine ridges, following the criteria proposed by Fernández-Fernández *et al.* (2019): (i) Boulders must be clearly part of the moraine ridge—embedded within it and unaffected by postglacial erosion processes such as landslides, debris flows, snow avalanches or rockfall. They must be located on the ridge crest to minimize the effect of snow cover. (ii) The selected lichen species must be sufficiently abundant to allow multiple measurements at each site. Thalli must be well-defined and not coalescent, as merging can hinder growth and measurement accuracy. (iii) Only the largest circular or elliptical thalli of the selected species, located on flat, horizontal boulder surfaces, were measured.

The species *Rhizocarpon geographicum* (L.) DC (hereafter RG) was selected for the measurements. At each measurement site, the boulder bearing the largest visible lichen within a 5-m radius was chosen. We adopted the 'largest single thallus' approach for RG, as previously used in lichenometric studies of moraines in Tröllaskagi (Caseldine 1983, 1985, 1987, 1991; Kugelmann 1991). High-resolution digital photographs of the most representative largest thalli were taken by the same researcher, using an Icelandic króna coin (21 mm diameter) placed parallel to the lichen surface as a graphic scale reference.

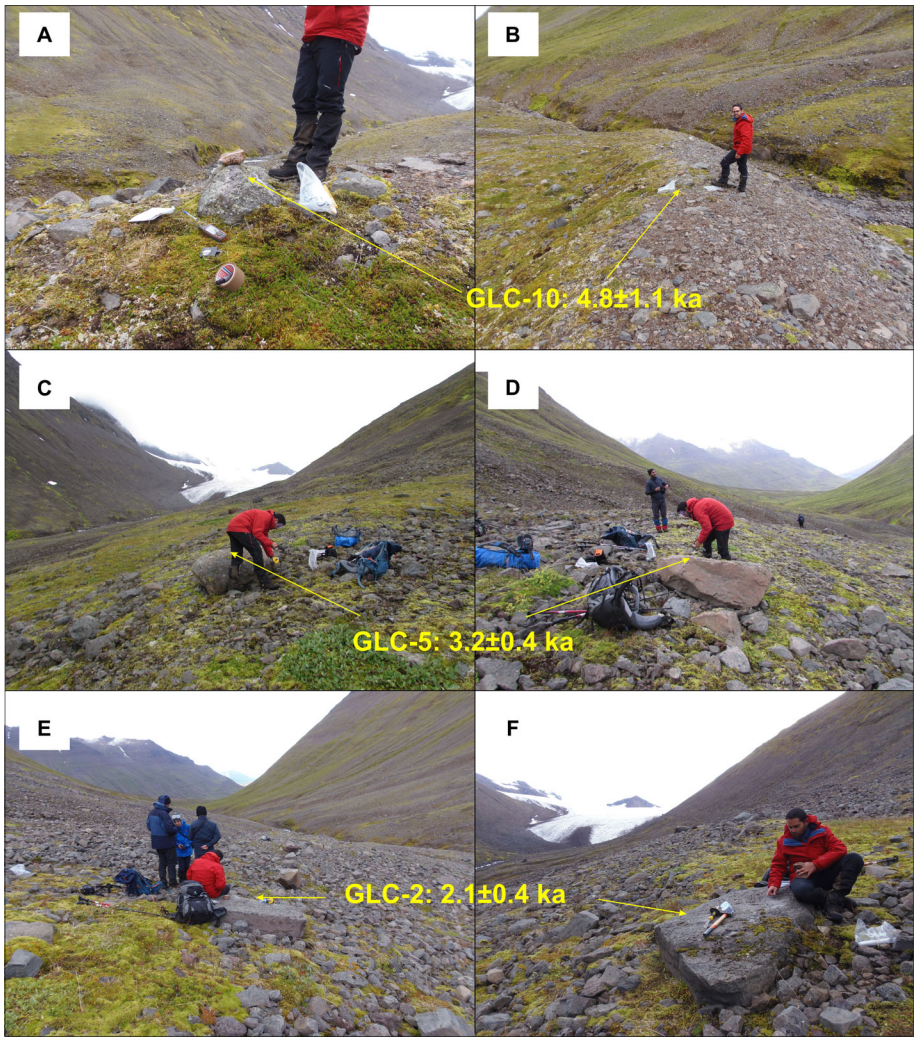

Fig. 4. Some examples of boulders sampled for CRE dating in well-preserved segments of the moraines and their results, taken in 2018. A, B. Segment of one of the Phase-3 moraines. C, D. Segment of Phase 3 moraine, close to Phase 4. E, F. A moraine segment of Phase-5. Photos of August 2018.

To minimize potential lens distortion, the photographs were taken so that both the lichen (on plain surfaces) and coin planes were centrally located and perpendicular to the lens's line of sight. Subsequently, images were scaled to real dimensions in ArcGIS, and thalli outlines were traced manually. Diameters were then automatically calculated as the smallest circle capable of circumscribing the thallus, representing the longest axis. We preferred this approach (Hooker & Brown 1977; McCarthy & Zaniewski 2001) to the standard direct measurement of lichens by means of a calliper for the following reasons: (i) it is a non-invasive alternative that does not exert any disturbance or alteration on the thalli; (ii) it is a permanent archive that avoid potential sources of error when recording measurements; (iii) taking easily scalable photos is faster than manual measurement, which allows surveying more sites (i.e. lichen thalli) in less time, enhancing sampling coverage; (iv) it allows further derived analysis such as lichen perimeter, surface, morphometric indexes, etc.; and (v) it reduces user-derived subjectivity and enhanced consistency so that the real longest axis (i.e. diameter of the smallest circumscribing circle) is always identified, which is not always ensured when using calliper. For these reasons, this approach can be considered even more reliable with no significant disadvantages (Bradwell 2010; Sancho *et al.* 2011, 2017). Error resulting from measuring lichens on digital photographs is unlikely to significantly affect the ages obtained; in fact, any unusual results are more likely due to the disappearance of lichens from the original colonizing population or to failure to identify the largest lichen at a given measurement site (see Osborn *et al.* 2015).

To infer the exposure age of the boulders, we applied a constant RG growth rate of 0.44 mm a^{-1}, consistent with previous work in Tröllaskagi

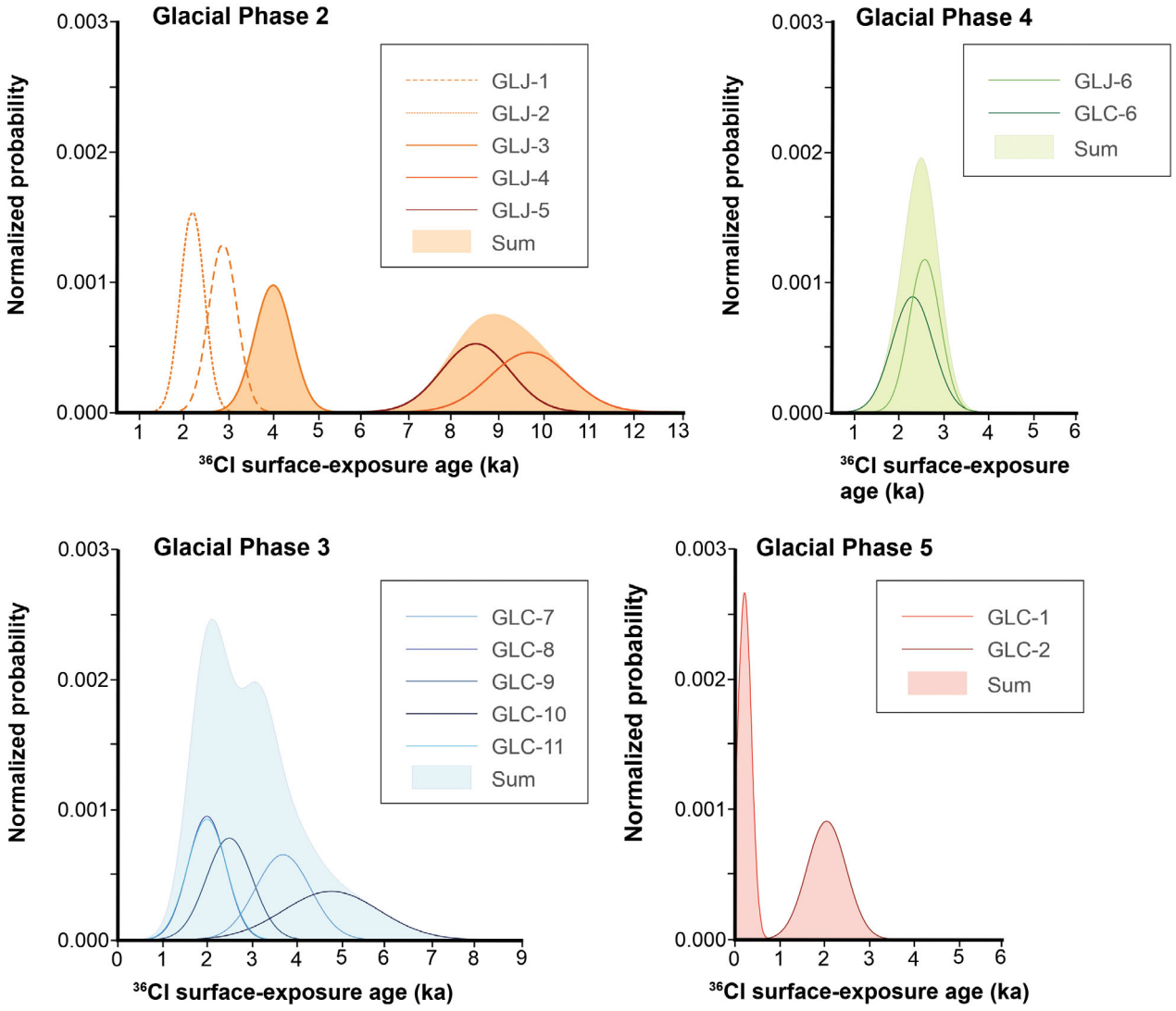

Fig. 5. Probability density plots of CRE ages for different chronostratigraphic units of Phases 1 to 5. In the text, it has been justified why the older ages are proposed as more likely, not the mean and median. The samples GLJ-1 and -2 have been considered as clear outliers.

(Häberle 1991; Kugelmann 1991; Fernández-Fernández *et al*. 2019). Applying a constant rate implies assuming that measured lichens are at their linear growth phase, therefore the derived ages should be taken carefully as minimum, especially for the older moraines (expected to be >100–150 years old). A lag time (ecesis interval) of 15–20 years was also considered, in line with values validated in nearby valleys (Fernández-Fernández *et al*. 2019). The resulting ages were evaluated by considering both the spatial distribution of lichen localities, the chronostratigraphical arrangement and the former glacier snout positions visible over historical aerial photographs (see above), which were used to constrain maximum and minimum exposure ages. The location of the lichen measurement sites and the results are presented in Table 5 and Figs 2 and 6.

Glacier reconstruction

Glacier reconstruction was performed following the procedures proposed by Benn & Hulton (2010), based on the reconstruction of equilibrium ice profiles supported on a physical-based model describing ice rheology and glacier flow (Van der Veen 1999), aiming to achieve a robust glacier reconstruction. This kind of model operates on completely ice-free areas, which is not the case of Gljúfurárdalur—it is currently occupied by a single corrie glacier, that is Gljúfurárjökull, accounting for 3.09 km^2 in total.

To obtain the bedrock topography, the ArcGIS toolbox 'VOLTA' (Volume and Topography Automation; James & Carrivick 2016) was run in the work interface of ArcMap (version 10.4). The toolbox models the spatial distribution of ice masses by assuming a perfect

Table 2. Chemical composition of the bulk rock samples before chemical treatment.

Sample name	CaO (%)	K_2O (%)	TiO_2 (%)	Fe_2O_3 (%)	SiO2 (%)	Na_2O (%)	MgO (%)	Al_2O_3 (%)	MnO (%)	Cl (ppm)	P_2O_5 (%)	Li (ppm)	B (ppm)	Sm (ppm)	Gd (ppm)	Th (ppm)	U (ppm)
GLJ-1	10.15	0.56	3.17	14.46	48.03	2.56	5.68	13.10	0.19	57.00	0.35	5.10	<2.00	7.27	7.22	1.43	0.43
GLJ-2	9.00	0.60	3.48	15.23	49.21	2.82	5.24	12.91	0.23	48.00	0.36	6.10	<2.00	7.96	8.16	1.77	0.53
GLJ-3	9.02	0.61	3.48	15.17	49.00	2.79	5.29	12.93	0.21	43.00	0.36	5.70	<2.00	7.59	7.81	1.82	0.51
Mean	9.39	0.59	3.38	14.95	48.75	2.72	5.40	12.98	0.21	49.33	0.36	5.63	<2.00	7.61	7.73	1.67	0.49
GLC-1	9.42	0.68	3.64	14.01	49.18	3.10	5.49	13.49	0.20	88.00	0.50	7.49	5.20	8.98	9.12	2.12	0.59
GLC-3	9.25	0.60	4.64	17.56	46.67	2.73	5.05	11.95	0.23	55.00	0.43	6.13	5.30	8.95	9.10	2.02	0.60
GLC-6	11.93	0.33	2.43	13.17	47.59	2.39	6.94	14.03	0.19	40.00	0.22	5.08	2.00	5.11	5.40	1.09	0.30
GLC-7	8.94	0.56	3.55	15.94	47.97	2.79	5.22	12.62	0.22	37.00	0.36	6.67	2.80	8.03	8.26	1.69	0.50
GLC-10	8.67	0.63	4.24	16.64	47.43	3.01	4.61	12.43	0.23	84.00	0.46	7.48	3.50	8.74	8.70	2.10	0.54
Mean	9.64	0.56	3.70	15.46	47.77	2.80	5.46	12.90	0.21	60.8	0.39	6.57	3.76	7.96	8.12	1.80	0.51

plasticity of ice. It only requires the glacier outlines and a digital elevation model (DEM). Glacier outlines were manually drawn through visual inspection of a (false infrared colour) Sentinel 2 satellite image (spatial resolution: 10 m) collected on the 30th August 2017, when the study area was mostly snow-free and close to the collection date of the satellite images from which the DEM was produced. We used the ArcticDEM (Porter *et al.* 2022, 2023), derived from stereo autocorrelation applied to overlapping pairs of high-resolution (0.3–0.5 m) optical satellite images (Maxar WorldView 1–3 and GeoEye-1). Aiming to avoid the potential impact of some local artefacts, the DEM was smoothed through the 'Focal Statistics' command in ArcMap, considering a rectangular 10x10 cell neighbourhood (statistics type: mean). Then, 'VOLTA' routines were applied in two steps: (1) drawing the centrelines of the current ice masses along the axis of the glacier tongue and tributary branches, and perpendicular to the contour lines; (2) calculating the ice thickness along the centrelines. The default tool parameters were used (ice density = 900 kg m^{-3}; effective slope limit = 30°; minimum slope limit = 4°). For more details of the full calculation process, see James & Carrivick (2016). Then, the ice thickness was interpolated from the ice centreline thickness points through an inverse distance weighted (IDW) routine in ArcGIS, and the resulting raster was subtracted from the current DEM to produce a bare-rock DEM.

Over this 'deglaciated' DEM, glacier reconstruction was conducted through the 'PalaeoIce 2.0' ArcGIS toolbox devised by Li (2023). It was built on the basis of a previous toolbox 'GlaRe' programmed by Pellitero *et al.* (2016) and includes several improvements in the different steps of the internal workflow; for more details, see Li (2023: p. 3–8). The 3D glacier reconstruction only required the ice-free DEM, the outline of Gljúfurárjökull and a flowline. The outline of the glacier during different ice-marginal positions was successfully reconstructed based on the moraine ridges identified on the foreland and subsequently included in the geomorphological map (Fig. 2). Flowlines were manually drawn from the position of the outermost moraines to the cirque headwall, following the valley and tributaries axis (talweg), and the path of the centrelines used in the previous step. The original flowline was then clipped for each glacial outline. We used the Python script 'Palaeo Ice Reconstruction With Palaeoice Outline(s)', which considers the outline derived from geomorphic evidence (i.e. lateral moraines) as 'target ice elevations' (see Li 2023) to adjust and optimize the distribution of the shear stress values along the flowlines. Lateral drag of valley sides on the movement of the glacier was considered through the calculation of the shape (f) factor, derived from automatically derived cross-sections along the main flowline and tributaries (see Paterson 1994; Benn & Hulton 2010). We also used aerial images to track the evolution of the surface debris cover from

Table 3. Concentrations of the ^{36}Cl target elements determined in splits taken after the chemical pre-treatment (first acid leaching).

Sample name	CaO (%)	K_2O (%)	TiO_2 (%)	Fe_2O_3 (%)	SiO_2 (%)	Na_2O (%)	MgO (%)	Al_2O_3 (%)	MnO (%)
GLJ-1	9.56±0.48	0.52±0.10	4.02±0.40	13.87±0.28	51.12±1.02	2.32±0.23	5.50±0.11	11.14±0.22	0.20±0.04
GLJ-2	8.15±0.41	0.63±0.13	4.19±0.42	15.19±0.30	51.93±1.04	2.65±0.27	4.76±0.48	11.50±0.23	0.23±0.05
GLJ-3	8.16±0.41	0.61±0.12	4.31±0.43	15.84±0.32	51.15±1.02	2.57±0.26	4.92±0.49	11.18±0.22	0.23±0.05
GLJ-4	8.27±0.41	0.56±0.11	4.45±0.45	16.66±0.33	50.31±1.01	2.54±0.25	4.87±0.49	11.37±0.23	0.23±0.05
GLJ-5	11.68±0.23	0.24±0.06	2.80±0.28	13.40±0.27	50.20±1.00	1.96±0.20	7.43±0.15	11.21±0.22	0.19±0.04
GLJ-6	9.22±0.46	0.46±0.11	4.14±0.41	16.84±0.34	49.89±1.00	2.26±0.23	5.88±0.12	10.83±0.22	0.25±0.05
GLC-1	8.31±0.42	0.65±0.13	4.12±0.41	14.68±0.29	51.46±1.03	2.53±0.25	5.65±0.11	10.94±0.22	0.22±0.04
GLC-2	9.20±0.46	0.66±0.13	5.17±0.26	16.76±0.34	49.15±0.98	2.30±0.23	5.89±0.12	10.64±0.21	0.23±0.05
GLC-5	8.10±0.41	0.64±0.13	4.72±0.47	15.52±0.31	51.85±1.04	2.66±0.27	4.56±0.46	11.54±0.23	0.23±0.05
GLC-6	11.38±0.23	0.33±0.07	3.04±0.30	13.20±0.26	50.18±1.00	2.06±0.21	7.02±0.14	11.41±0.23	0.20±0.04
GLC-7	8.18±0.41	0.61±0.12	4.40±0.44	15.59±0.31	52.04±1.04	2.64±0.26	4.66±0.47	11.47±0.23	0.22±0.04
GLC-8	9.62±0.48	0.47±0.09	4.21±0.42	13.59±0.27	52.72±1.05	2.26±0.23	5.41±0.11	10.70±0.21	0.19±0.04
GLC-9	8.13±0.41	0.62±0.12	4.21±0.42	15.63±0.31	52.50±1.05	2.55±0.25	4.90±0.49	11.04±0.22	0.23±0.05
GLC-10	7.90±0.39	0.62±0.12	4.93±0.49	17.55±0.35	50.13±1.00	2.61±0.26	4.79±0.48	10.60±0.21	0.24±0.05
GLC-11	8.96±0.45	0.51±0.10	4.12±0.41	16.32±0.33	49.96±1.00	2.32±0.23	5.63±0.11	10.77±0.22	0.23±0.05

1946 CE to the present day (Paul *et al.* 2004). We mapped the debris surfaces through manual digitization, supported by visual analysis of the ice-marginal positions of these areas using GIS software. The data calculated for all glacier ice-marginal positions are summarized in the Table 6 and Figs 7, 8.

Equilibrium-line altitude (ELA) calculation

ELA was calculated for the reconstructed ice-marginal positions through the 'ELA calculation' toolbox developed by Pellitero *et al.* (2015); it only requires the DEM of the (reconstructed) glacier and produces a plain-text file with the ELA associated with the different methods (AA, area altitude; AAR, accumulation area ratio; AABR, area altitude balance ratio; MGE, median glacier elevation) and the *shapefiles* (.shp) of the corresponding glacier contours. We chose the AAR method, which needs a detailed knowledge of glacier surface hypsometry (i.e. distribution of surface as a function of elevation) and relies on a relationship of constant ratio between the glacier accumulation area and the whole glacier surface (i.e. the AAR). We used an AAR = 0.65, widely used worldwide (Meier & Post 1962; Porter 2000). From current and past ELA estimates (i.e. ELA shift, ΔELA), a modern-day lapse rate of 0.66 °C 100 m^{-1} for Tröllaskagi (Fernández-Fernández *et al.* 2017) and assuming that precipitation has remained constant throughout the Holocene, we have estimated minimum past temperature anomalies (ΔT) relative to present-day values (Eqn. 1; see Sutherland 1984):

Table 4. ^{36}Cl CRE dating results. Numbers in italics correspond to the internal (analytical) uncertainty at 1σ level. * = Outlier.

Glacial phase	Sample name	Sample weight (g)	Mass of Cl in spike (mg)	^{35}Cl/^{37}Cl	^{36}Cl/^{35}Cl (10^{-14})	Cl in sample (ppm)	^{36}Cl (10^4 atoms g^{-1})	^{36}Cl CRE age (ka)
Phase 2	GLJ-1	73.22	1.805	14.866±0.288	5.700±0.357	8.4±0.5	2.818±0.198	2.9±0.3 (*0.2*)
Phase 2	GLJ-2	73.76	1.813	9.519±0.174	3.719±0.285	15.7±0.9	2.104±0.188	2.2±0.3 (*0.2*)
Phase 3	GLJ-4	81.78	1.815	7.303±0.172	6.203±0.356	21.8±1.4	3.920±0.265	4.0±0.4 (*0.3*)
Phase 3	GLC-5	67.70	1.810	8.732±0.181	4.529±0.371	19.1±2.3	3.126±0.295	3.2±0.4 (*0.3*)
Phase 3	GLC-7	69.99	1.809	11.756±0.654	5.252±0.706	11.8±1.5	3.066±0.434	3.7±0.6 (*0.5*)
Phase 3	GLC-8	65.47	1.814	30.145±0.153	3.511±0.645	3.6±0.4	1.763±0.340	2.0±0.4 (*0.4*)
Phase 3	GLC-9	71.20	1.807	12.246±0.117	3.843±0.681	10.9±1.3	2.151±0.400	2.5±0.5 (*0.5*)
Phase 3	GLC-10	81.32	1.817	4.945±0.153	5.129±0.907	50.2±7.1	5.229±1.047	4.8±1.1 (*1.0*)
Phase 3	GLC-11	83.69	1.812	4.386±0.117	2.142±0.288	70.5±10.3	2.682±0.466	2.0±0.4 (*0.4*)
Phase 4	GLJ-6	84.90	1.826	4.716±0.101	3.185±0.238	56.1±4.5	3.287±0.321	2.6±0.3 (*0.3*)
Phase 4	GLC-6	87.27	1.806	8.426±0.173	4.637±0.772	15.6±1.9	2.531±0.446	2.3±0.5 (*0.4*)
Phase 5	GLC-1	81.54	1.794	4.595±0.123	0.538±0.132	61.3±8.7	0.565±0.167	0.20±0.2 (*0.2*)
Phase 5	GLC-2	84.75	1.794	3.107±0.054	2.338±0.289	75.9±12.7	3.077±0.545	2.1±0.4 (*0.4*)
Outlier	GLJ-3	75.83	1.820	8.955±0.088	14.304±0.590	16.8±0.9	8.819±0.409	9.7±0.9 (0.5)*
Outlier	GLJ-5	89.57	1.814	11.353±0.263	19.533±0.734	10.0±0.6	9.172±0.384	8.5±0.8 (0.4)*
	Blanks[1]					Total atoms Cl (10^{17})	Total atoms ^{36}Cl (10^4)	
	BK-1		1.800	297.029±11.372	0.545±0.097	2.941±0.220	16.981±3.034	
	BK-2		1.794	178.193±3.811	0.169±0.057	2.901±0.363	5.227±1.753	

[1]BK-1 was processed with samples GLJ-1 to GLJ-6; BK-2 was processed with samples GLC-1 to GLC-11.

Table 5. Sizes of the largest lichen at the lichen stations in Gljúfurárjökull and surface dates. The age of the lichen was deduced according to the period of ecesis (15–20 years) that previous literature has observed for this species in this area. See explanation in the text.

Lichen locality	GPS location		Glacial phase or/ and terminal position (TP)	*Rhizocarpon geographicum*	Surface date from growth rate (year)	
	Latitude (N)	Longitude (W)		Min. circ. diameter (mm)	15-year col.	20-year col.
GLJUF-1	65°44′6.60″	18°38′54.00″	Phase 1	—[1]	—[1]	
GLJUF-2	65°44′2.22″	18°38′52.26″	Phase 3	40.4[2]	1907	1902
GLJUF-3	65°43′59.16″	18°38′48.60″	Phase 3	48.3[2]	1889	1884
GLJUF-4	65°43′57.84″	18°38′49.62″	Phase 4	73.6[2]	1832	1827
GLJUF-5	65°43′51.42″	18°38′49.86″	Phase 5	—[1]	—[1]	
GLJUF-6	65°43′50.70″	18°38′51.48″	Phase 5	58.4[2]	1866	1861
GLJUF-7	65°43′46.56″	18°38′53.04″	Phase 6	41.8	1904	1899
GLJUF-8	65°43′45.30″	18°38′52.38″	Phase 6	46.4	1894	1889
GLJUF-9	65°43′43.08″	18°38′51.72″	Phase 7	35.9	1917	1912
GLJUF-10	65°43′39.60″	18°38′49.86″	TP 8	21.7	1950	1945
GLJUF-11	65°43′37.20″	18°38′53.10″	TP 9	16.5	1962	1957
GLJUF-12	65°43′34.83″	18°38′52.68″	TP 10–11	6.4	1984	1979
GLJUF-13	65°43′29.28″	18°38′55.32″	TP 13	—[1]	—[1]	

[1]Dash '—' indicates that no lichen was found.
[2]Unreliable according to geomorphological position.

$$\Delta T\ [^{\circ}\mathrm{C}] = \Delta \mathrm{ELA}\ [\mathrm{m}] \times 0.66\ [^{\circ}\mathrm{C}\ 100\,\mathrm{m}^{-1}] \quad (1)$$

ELA results and (minimum) temperature estimations are presented in Table 7.

Results

Geomorphological and ice-marginal position evolution at Gljúfurárdalur and exposure sampling strategy

Based on the 2019 aerial orthophoto and field observations, only limited segments of the moraines previously identified by Caseldine (1983, 1985) could be recognized. This is largely due to substantial geomorphic changes in the glacier foreland, primarily caused by frequent debris flows and snow avalanches that may have eroded or buried the moraines. Consequently, only the best-preserved sections were mapped during fieldwork. It is important to note that the most prominent moraine ridges, which have served to reconstruct former ice-marginal positions, were not always suitable for dating by lichenometry or CRE methods. Although these moraines often contain a considerable number of boulders, many have been reworked or covered by slope-derived deposits, rendering them unsuitable for surface exposure dating.

Only isolated and well-preserved moraine ridges, which maintain their original morphology and surface boulders, were considered for sampling. Lichenometric and CRE sampling sites were selected based on this criterion. Importantly, geomorphological analysis confirms that the sampled sites have not been buried by slope-derived sediments.

We identified and reconstructed seven distinct ice-marginal positions (1–7), based on the morphology of moraine ridges (Figs 2, 7, 8). Some positions were defined solely from aerial photographs, and in these cases, it is unclear whether the glacier was advancing, retreating or stationary. Other positions are delineated by frontal and lateral moraines, indicating a stabilized glacier front following an advance—these are referred to as distinct 'glacial phases'.

- Ice-Marginal Position 1 (Glacial Phase 1)—This is the outermost moraine, visible in both the orthophoto and field observations. It is heavily covered by debris flow deposits and recent snow avalanche material. A well-defined frontal and eastern section stands out in the topography, although it is mostly overlain by slope debris. No original moraine boulders were found on the surface, precluding CRE and lichenometric dating (GLJUF-1)—The moraine ridge is approximately 5 m high and 8–10 m wide.
- Ice-Marginal Position 2 (Glacial Phase 2)—This position is delineated by moraine ridges affected by slope processes. However, in the central sector west of the river channel, well-preserved boulders are present. CRE samples GLJ-1, GLJ-2 and GLJ-3 were collected here, and lichen locality GLJUF-2 was measured. The ridge is ∼3 m in relief and ∼150 m inboard of Phase 1.
- Ice-Marginal Position 3 (Glacial Phase 3)—Defined by a series of closely spaced, well-preserved moraine ridges at the valley bottom, west of the river channel. These ridges are unaffected by slope processes. Additional well-preserved ridges are located slightly further up-valley. CRE samples collected include GLJ-4, GLJ-5, GLC-5, GLC-7, GLC-8, GLC-9, GLC-10 and GLC-11, and the lichen locality GLJUF-2 was measured. The ridge is ∼3 m high and ∼100 m inboard of Phase 2.

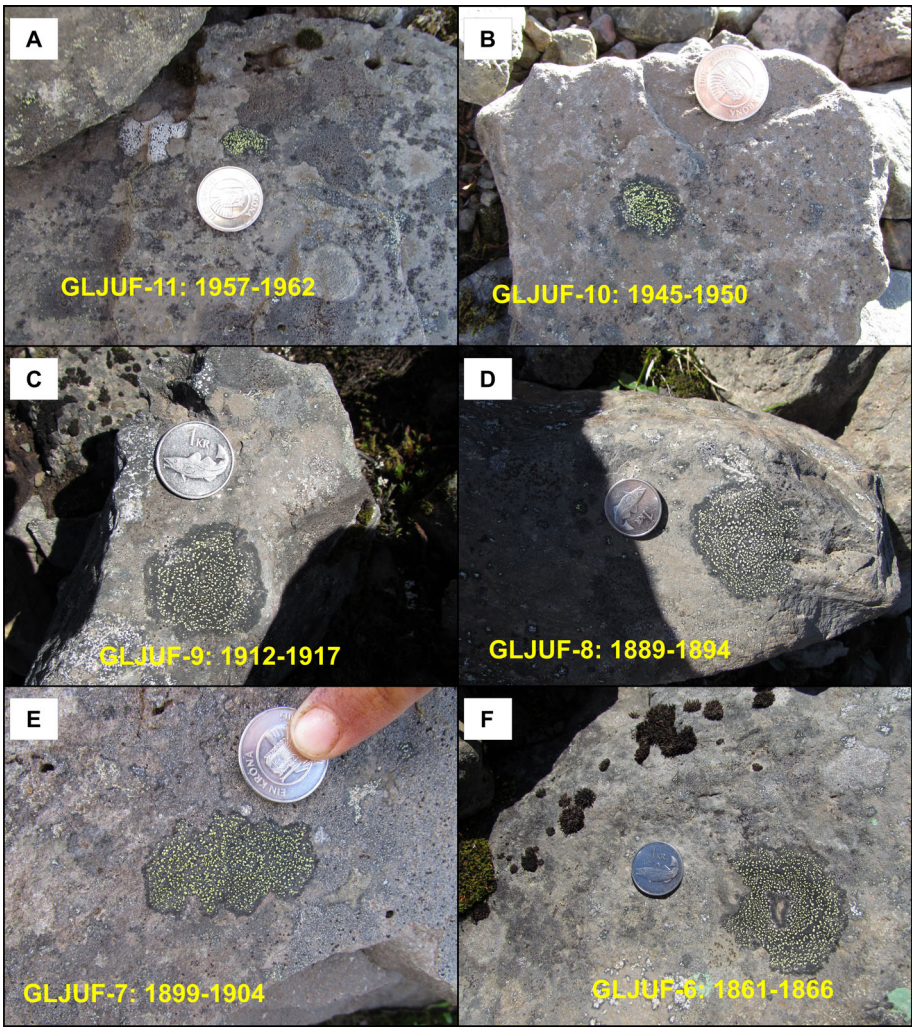

Fig. 6. A–F. Some examples of the boulders where the largest thalli have been found in each of the glacier boundaries, applying the rate of 44 mm a^{-1}. For the first two, their age fully coincides with that deduced from the 1960 to 1945 CE aerial photos. The others follow a logical order of size as they are located further away from the current glacier front. Photos of August 2014.

- Ice-Marginal Position 4 (Glacial Phase 4)—This phase is defined by the best-preserved moraines situated far from slope activity, west of the river channel. Two boulders (GLJ-6 and GLC-6) were sampled for CRE, and two lichen localities (GLJUF-3 and -4) were measured. The moraine ridge is ∼4 m in relief and ∼150 m inboard of Phase 3.
- Ice-Marginal Position 5 (Glacial Phase 5)—Moraine ridges are preserved only in a limited area at the valley bottom, west of the river. Between Phases 4 and 5, a large area has been swept by debris flows, obliterating any intermediate moraines. Two boulders (GLC-1 and GLC-2) were sampled for CRE, and two lichen localities (GLJUF-5 and -6) were established. The ridge is ∼3 m high and ∼150 m inboard of Phase 4.
- Ice-Marginal Position 6 (Glacial Phase 6)—A moraine ridge marks the inner position of Phase 5. Due to their likely young age, no CRE samples were taken, but lichenometric measurements were made in two localities (GLJUF-7 and -8).
- Ice-Marginal Position 7 (Glacial Phase 7)—Located ∼130 m up-valley from Phase 6, there is a moraine, which rises ∼3.5 m above the valley floor. Lichenometric measurements were conducted in one locality (GLJUF-9).

Beyond Phase 7, although well-preserved moraines continue to be mapped, additional ice-marginal positions (8–16) were delineated based on glacier outlines visible in aerial orthophotos (1946, 1960, 1985, 1994, 2000, 2016 and 2019) and medium-resolution satellite imagery (2005, 2017). To support lichenometric calibration, additional measurements were taken along these younger positions (GLJUF-10, -11, -12 and -13) (Figs 2, 7, 8).

Table 6. Glacier length, snout position changes, area, volume and associated variations between consecutive stages. The asterisk indicates that glacier length and snout position changes are measured along the main flowline used for glacier reconstruction.

Glacial Phase/Ice terminal position (TP)	Inferred age	Length* (m)	Δ* (m)	Area (km^2)	Area Δ (%)	Volume (km^3)	Volume Δ (%)	Min. altitude (m a.s.l.)	Min. altitude Δ (m)	Covered by debris (ha)	Covered by debris (%)
Phase 1	>2.6±0.5 ka	4145	—	3.939	—	0.290	—	484.82	—		
Phase 2	2.6±0.5 ka	4025	−120	3.886	−1.334	0.292	+0.559	494.70	9.88		
Phase 3	3.2±1.1 ka	3938	−87	3.831	−1.431	0.286	−2.037	502.72	8.02		
Phase 4	2.5±0.2 ka	3773	−165	3.639	−4.998	0.265	−7.183	512.88	10.16		
Phase 5	From 2.1 ka to a few hundred years	3615	−158	3.565	−2.029	0.262	−0.988	524.51	11.63		
Phase 6	1899/1904 CE	3433	−182	3.499	−1.846	0.258	−1.802	543.32	18.80		
Phase 7	1912/1917 CE	3334	−99	3.440	−1.690	0.250	−2.855	549.63	6.31		
TP 8	1946 CE	3280	−55	3.403	−1.071	0.251	+0.180	556.15	6.52	6.11	1.16
TP 9	1960 CE	3126	−154	3.344	−1.753	0.252	+0.522	573.40	17.25		
TP 10	1985 CE	3010	−117	3.271	−2.187	0.246	−2.233	587.20	13.81	4.80	1.34
TP 11	1994 CE	3030	+20	3.277	+0.189	0.244	−0.857	585.40	−1.80	2.60	0.74
TP 12	2000 CE	3006	−24	3.256	−0.639	0.241	−1.507	589.07	3.67		
TP 13	2005 CE	2927	−79	3.209	−1.441	0.241	+0.029	598.33	9.25		
TP 14	2016 CE	2802	−125	3.164	−1.410	0.241	+0.103	612.85	14.52	5.50	1.65
TP 15	2017 CE	2799	−3	3.108	−1.757	0.221	−8.448	613.75	0.90		
TP 16	2019 CE	2788	−11	3.089	−0.624	0.224	+1.621	617.89	4.14	7.56	2.25

Chronology of the glacier ice-marginal positions

Chronology of the phases of Gljúfurárjökull: ^{36}Cl CRE dating. – The CRE ages obtained from moraine boulders exhibit a general trend from older to younger across the first five glacial phases for which CRE data are available (Table 5, Fig. 2), with ages ranging from 9.7±0.9 to 0.2±0.2 ka. Despite notable scatter within the age groups of each phase, 12 out of the 15 boulder ages fall within the interval of approximately 4.5 to 2 ka. We therefore consider two interpretative approaches: (i) excluding the most obvious outliers and calculating arithmetic mean exposure ages and standard deviations for each phase (Balco 2020); and (ii) assigning the oldest boulder age to each corresponding glacial phase (cf. Putkonen & Swanson 2003; Briner *et al.* 2005; Putkonen *et al.* 2008; Heyman *et al.* 2011).

- Glacial Phase 1—This phase corresponds to the oldest moraine, for which no reliable boulders were available for exposure dating. As such, it was not sampled. We hypothesize that this moraine predates the mean age of Phase 2 (>2.6±0.5 ka; see Discussion) or possibly even predates the oldest sample of Phase 2 (>9.7±0.9 ka).
- Glacial Phase 2—Three boulders were sampled from this phase, yielding exposure ages of 2.9±0.3 ka (GLJ-1), 2.2±0.3 ka (GLJ-2) and 9.7±0.9 ka (GLJ-3). The age spread may reflect inheritance in the oldest sample and/or post-depositional processes such as moraine collapse, which could have exposed previously buried boulders and produced anomalously young ages. Given that the oldest sample is several thousand years older than the others, it is considered an outlier and excluded. The remaining two samples have overlapping 2σ analytical uncertainties, and we calculate a tentative arithmetic mean and standard deviation of 2.6±0.5 ka ($n = 2$). This may represent a minimum age, as it slightly postdates the mean age of Glacial Phase 3, although both ages overlap within uncertainty.
- Glacial Phase 3—Eight boulders were dated, yielding exposure ages of 4.0±0.4 ka (GLJ-4), 8.5±0.8 ka (GLJ-5), 3.2±0.4 ka (GLC-5), 3.7±0.6 ka (GLC-7), 2.0±0.4 ka (GLC-8), 2.5±0.5 ka (GLC-9), 4.8±1.1 ka (GLC-10) and 2.0±0.4 ka (GLC-11). The 8.5 ka age is significantly older than the others and is interpreted as an outlier, likely due to inheritance. Excluding this sample, the arithmetic mean and standard deviation of the remaining seven boulders are 3.2±1.1 ka ($n = 7$).
- Glacial Phase 4—Two boulders from this phase yielded exposure ages of 2.6±0.3 ka (GLJ-6) and 2.3±0.5 ka (GLC-6), resulting in a mean age of 2.5±0.2 ka ($n = 2$).
- Glacial Phase 5—Two samples yielded divergent exposure ages: 2.1±0.4 ka (GLC-2) and 0.2±0.2 ka (GLC-1). Due to the inconsistency and lack of additional data, we tentatively assign Glacial Phase 5 to a time range between 2.1 ka and a few hundred years ago.

Chronology of the glacial phases of Gljúfurárjökull according to lichenometric dating. – During fieldwork, we aimed to conduct lichen measurements at the same localities established over 40 years ago in previous studies by Caseldine (1983, 1985, 1987, 1991), in order to enable comparative analysis. However, the lichen distribution patterns have changed significantly since those earlier surveys, particularly on moraines corresponding

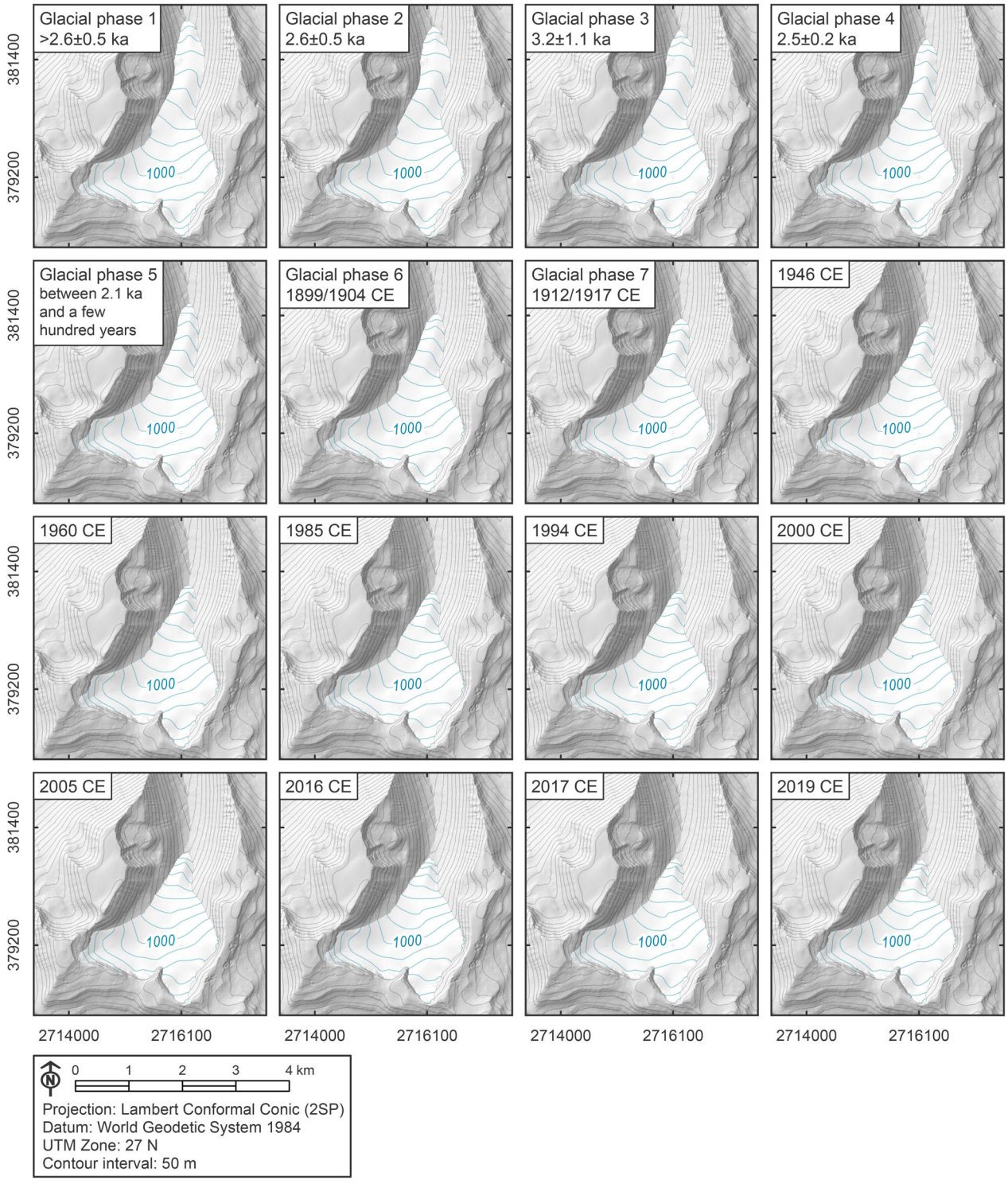

Fig. 7. Extent of Gljúfurárjökull during the 16 glacier terminal positions identified in this work and proposed chronology.

to the oldest glacier phases. Contrary to expectations, the thalli were often smaller than reported previously—or entirely absent. We interpret this primarily as the result of snow avalanche activity and snow kill.

We measured the largest visible thallus at each site to estimate the age of each moraine (Table 5). However, the lichenometric results obtained for Glacial Phases 1 through 5 do not follow a consistent or logical

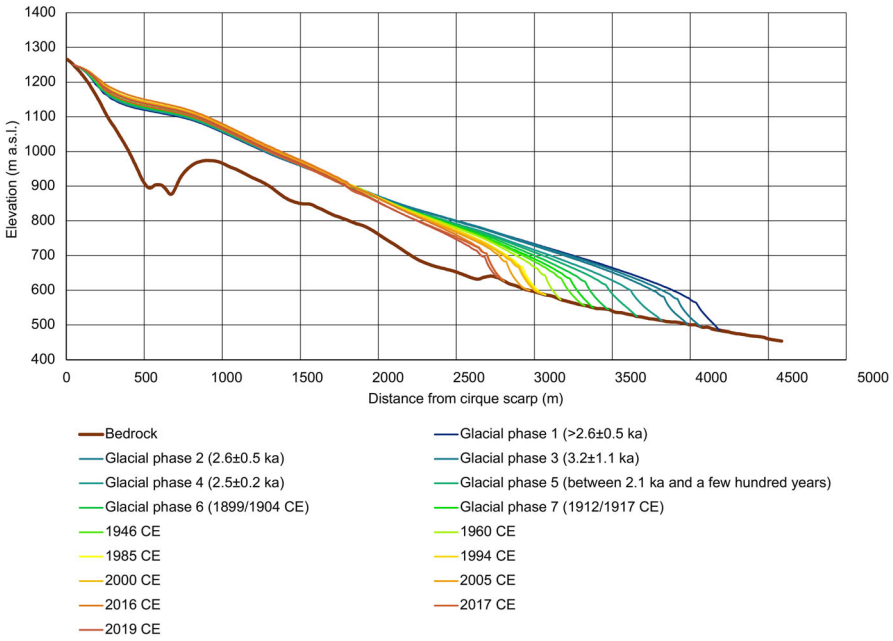

Fig. 8. Transect of Gljúfurárjökull during the 16 glacier terminal positions in this work and proposed a chronology.

chronological pattern. For instance, at Phase 5, locality GLJUF-6 yielded a lichenometric age of 1861/1866 CE, yet it lies very close to boulders with CRE exposure ages of 2.1±0.4 ka (GLC-2) and 0.2±0.2 ka (GLC-1). In contrast, the nearby locality GLJUF-5 had no lichen thalli at all, highlighting the high degree of environmental instability in this area. Glacial Phase 1—the oldest mapped position—lacks any visible thalli (e.g. locality GLJUF-1). Meanwhile, the remaining Phases (2, 3, 4 and 5) display lichenometric ages ranging from 1827 to 1907 CE, which are inconsistent with the CRE ages and do not correlate logically with the spatial order of the moraines. Paradoxically, older lichen ages appear on moraines situated further from the current glacier terminus.

- Glacial Phase 6—Lichen localities GLJUF-8 and GLJUF-7, established near the Phase 6 moraine,

Table 7. Equilibrium-line altitudes, variations from consecutive stages and inferred summer temperature depression compared to present-day values.

Glacial phase/ice terminal position (TP)	Inferred age	Equilibrium-line altitude (m a.s.l.)				Summer temperature depression (°C)	
		AAR = 0.65	Δ (m)	AABR = 1.5	Δ (m)	From AAR	From AABR
Phase 1	>2.6±0.5 ka	914	—	922	—	−0.5	−0.5
Phase 2	2.6±0.5 ka	924	+10	932	+10	−0.5	−0.4
Phase 3	3.2±1.1 ka	927	+3	935	+3	−0.4	−0.4
Phase 4	2.5±0.2 ka	947	+20	945	+10	−0.3	−0.3
Phase 5	From 2.1 ka to a few hundred years	954	+7	957	+12	−0.3	−0.3
Phase 6	1899/1904 CE	958	+4	961	+4	−0.2	−0.2
Phase 7	1912/1917 CE	964	+6	967	+6	−0.2	−0.2
TP 8	1946 CE	971	+7	969	+2	−0.1	−0.2
TP 9	1960 CE	973	+2	981	+12	−0.1	−0.1
TP 10	1985 CE	982	+9	985	+4	−0.1	−0.1
TP 11	1994 CE	980	−2	983	−2	−0.1	−0.1
TP 12	2000 CE	979	−1	987	+4	−0.1	−0.1
TP 13	2005 CE	983	+4	991	+4	−0.1	0.0
TP 14	2016 CE	992	+9	995	+4	0.0	0.0
TP 15	2017 CE	988	−4	991	−4	0.0	0.0
TP 16	2019 CE	992	+4	995	+4	0.0	0.0

yielded ages of 1894/1889 and 1899/1904 CE (RG), respectively. Based on these results, we propose that Phase 6 corresponds to a glacier advance occurring between 1899 and 1904 CE (Table 5).

- Glacial Phase 7—No suitable lichen sites were found directly on the moraine delimiting Glacial Phase 7. The most representative site is GLJUF-9, located just in front of (but close to) the limit of Ice-Marginal Position 8, as identified in the 1946 CE aerial photograph. Lichenometric dating at GLJUF-9 yielded an age of 1912/1917 CE (RG). This date would be plausible if Ice-Marginal Position 8 corresponds to a glacial advance over a surface that had been ice free for approximately 40 years.

The most recent ice-marginal positions of Gljúfurárjökull throughout historical aerial photographs and satellite images and lichenometry dating. – The most recent glacier marginal positions, dating from 1946 onwards, have been delineated using historical aerial photographs and validated through lichenometric dating.

- Ice-Marginal Position 8 (1946 CE)—This position corresponds to the glacier extent visible in the 1946 aerial photograph. Lichen locality GLJUF-10 is located between Ice-Marginal Positions 8 and 9 and yielded lichenometric dates of 1945/1950 CE (RG). These results fall between the dates of the adjacent glacier positions (1946 and 1960 CE), supporting the reliability of the lichenometric method in this case.
- Ice-Marginal Position 9 (1960 CE)—This glacier marginal position was mapped using a 1960 aerial photograph and corresponds to a prominent moraine ridge, where lichen locality GLJUF-11 is situated. The locality produced lichenometric dates of 1957/1962 CE (RG). These results are consistent with the mapped ice position and support the chronological validity of the RG method in this context.
- Ice-Marginal Positions 10 (1985 CE) and 11 (1994 CE)—Analysis of aerial photographs indicates that the glacier advanced between 1985 and 1994, as evidenced by the 1994 ice extent exceeding that of 1985 (see above). Lichen locality GLJUF-12, located between these two positions, yielded dates of 1979/1984 CE (RG). These results suggest a low ecesis interval, estimated at approximately 15 years for RG.
- Ice-Marginal Positions 14, 15 and 16 (2016–2019 CE)—These positions, derived from aerial imagery taken in 2016, 2017 and 2019, show only minor retreat between 2016 and 2019. Lichen locality GLJUF-13, located ~20 m outside the 2016 moraine (Ice-Marginal Position 14), showed no visible lichen thalli in 2018 suggesting that colonization was still ongoing.

Evolution of length, extent and volume of Gljúfurárjökull

To assess glacier magnitude changes, we included the proposed ages for each ice-marginal position (Tables 6, 7). During the maximum ice extent (Glacial Phase 1), as indicated by the outermost moraines, Gljúfurárjökull extended over 4 km in length, covered an area of 3.9 km^2 and contained approximately 0.29 km^3 of ice. Since then, the glacier has retreated more than 1.3 km (a 32% reduction in length) and has lost 21.6% of its surface area and 22.7% of its ice volume (Table 6).

Overall, the glacier shows a long-term retreating trend. However, aerial photo analysis reveals a temporary advance between ice-marginal positions 10 (1985) and 11 (1994), with the snout progressing by 20 m. The greatest surface area losses occurred between ice-marginal positions 4, 5 and 10, ranging from 2% to 5% (Table 6). In terms of ice volume, the largest decreases were observed during transitions to ice-marginal positions 4, 7 and 15, with losses ranging from ~3% to over 8%.

Interestingly, despite the general retreat, some ice-marginal positions show slight ice volume gains (Table 6). We attribute these anomalies to the behaviour of the 'PalaeoIce' toolbox, particularly its optimization of shear stress distribution along flowlines. It likely performs better when modelling strongly contrasting glacier extents (e.g. Last Glacial Maximum vs. Little Ice Age). Therefore, we consider these minor volume increases, especially in smaller glacier extents, to fall within the toolbox's uncertainty margins.

The proportion of debris-covered ice was substantial during retreat phases—0.066 km^2 in 1946, representing 1.68% of the glacier area. This proportion decreased during the 1994 advance (0.026 km^2; 0.75%) and rose again as retreat resumed, increasing from 1.65% in 2019 to 2.25%.

Evolution of equilibrium-line altitudes (ELAs) of Gljúfurárjökull

The application of the AAR method resulted in equilibrium line altitudes (ELAs) ranging from 914 to 992 m a.s.l., whereas the AABR method yielded slightly higher values—by approximately 3 to 8 m—ranging from 922 to 995 m a.s.l. (Table 7). Both methods reveal a long-term increasing trend in ELA, corresponding to shifts of +78 m (AAR) and +73 m (AABR), respectively. The most pronounced ELA increases between successive ice-marginal positions occurred at transitions to positions 2, 4, 10 and 14 in the AAR reconstructions (approximately +10 to +20 m), and to positions 2, 4, 5 and 9 in the AABR reconstructions (+10–12 m). Similar to the behaviour observed in terminus position changes, a slight ELA decrease is evident between ice-marginal positions 10 and 11, coinciding with a glacier advance. Minor decreases are also observed at transitions to other

ice-marginal positions (e.g. 12 and 15; see Table 2), which are interpreted as artefacts of the glacier reconstruction process and reflect the inherent uncertainties of both methods due to their differing assumptions and sensitivity.

Using the ELA depressions relative to the present-day ELA, and applying the local lapse rate (Eqn. 1), we estimated minimum summer temperature anomalies compared to modern climate conditions. Assuming that long-term precipitation remained constant, the ELA depressions of –78 m (AAR) and –73 m (AABR) inferred for Glacial Phase 1 would indicate a summer cooling of approximately 0.5 °C. As expected, the temperature depression (ΔT) decreases progressively as the glacier retreated: approximately −0.5 °C for phases 1–2; −0.4 °C for Glacial Phase 3; −0.3 °C for phases 4–5; −0.2 °C for ice-marginal positions 6–8; −0.1 °C for ice-marginal positions 9–13; and values close to present-day conditions (ΔT ≈ 0 °C) for ice-marginal positions 14–16.

Discussion

Analysis of the validity of the results about glacial phases and their chronology

The foreland of Gljúfurárjökull exhibits a complex moraine system, comparable to those of other debris-free glaciers in Tröllaskagi, such as Tungnahryggsjökull (Fernández-Fernández *et al*. 2019). However, in this valley, slope processes are particularly active (Fig. 9). Debris flows have destroyed large portions of the moraine ridges or buried them under sediment. Moreover, snow avalanches occur frequently, often displacing or overturning moraine boulders, as confirmed by geomorphological analyses during multiple field campaigns. This dynamic is also evident when comparing our observations with geomorphological maps produced over 40 years ago (Caseldine 1983, 1985, 1987; Caseldine & Cullingford 1981).

Despite these challenges, it has been possible to delineate isolated, well-preserved sections of moraine ridges, which have allowed us to identify seven glacier phases predating the oldest available aerial photograph (1946 CE; see Figs 2, 7, 8).

All our CRE boulder ages fall within the Holocene, but are associated with scatter and partly not consistent with the geomorphic stratigraphy, preventing us from unambiguously assigning a conclusive chronology to the moraines. For instance, within Glacial Phase 2, some boulders yield ages around 9 ka, while others in the same geomorphological unit date to approximately 2 ka. A likely explanation is that the boulder ages are affected by a combination of post-depositional processes (e.g. Applegate *et al*. 2010; Heyman *et al*. 2011; Palacios *et al*. 2019) and nuclide inheritance, the latter phenomenon being particularly often documented in Arctic settings (e.g. Levy *et al*. 2014; Schweinsberg *et al*. 2019; Søndergaard *et al*. 2019; Larsen *et al*. 2021).

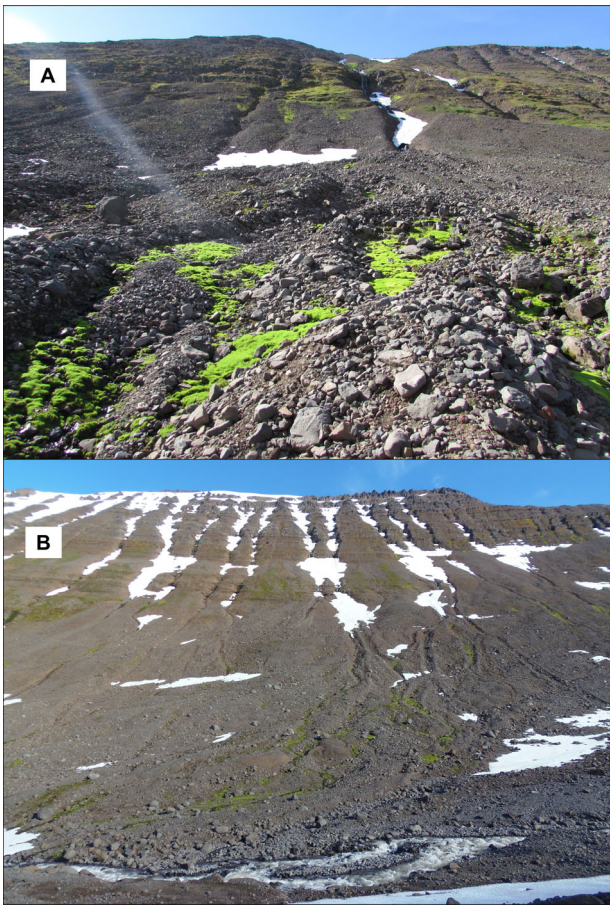

Fig. 9. Examples of valley sectors previously occupied by Gljúfurárjökull, where glacial landforms have been intensively dismantled by post-glacial erosional processes. A. Slope previously occupied by moraines, transformed by debris flows and snow avalanches. B. Fans of several generations of debris flows, partially deflected by lateral moraines. Remnants of snow avalanches can be seen in both photos. Photos from August 2014.

Applying the principle of relying on the oldest exposure ages within a moraine boulder age population (Putkonen & Swanson 2003; Briner *et al*. 2005; Putkonen *et al*. 2008; Heyman *et al*. 2011), would yield the following chronology for Gljúfurárjökull: Glacial Phase 1: >9.1±0.8 ka; Glacial Phase 2: 9.1±0.8 ka; Glacial Phase 3: 4.8±1.1 to 3–2±0.4 ka; Glacial Phase 4: 2.4±0.4 ka; and Glacial Phase 5: 2.1±0.4 ka to a few centuries ago. In this scenario, phases 1 and 2 would be of Early Holocene age or older. However, as only 2 out of 15 boulder ages are significantly older than ∼4.8 ka (GLJ-3, 9.7±0.9 ka; GLJ-5, 8.5±0.8 ka), it is most likely that they are outliers affected by several thousand years of inheritance. Therefore, we have chosen to estimate mean exposure ages for each phase, after excluding these outliers, as a more robust approach. The resulting ages are: Glacial Phase 1: no samples, but likely >2.6±0.5 ka; Glacial Phase 2: 2.6±0.5 ka ($n = 2$, minimum age?); Gla-

cial Phase 3: 3.2±1.1 ka ($n = 7$); Glacial Phase 4: 2.5±0.2 ka ($n = 2$); Glacial Phase 5: between 2.1 ka and a few hundred years ago. Notably, when considering uncertainties, phases 2, 3 and 4 overlap, all centring around a minimum age of ∼2.5 ka (Fig. 5).

Later ice-marginal positions were dated using lichenometry and the temporal context provided by aerial and satellite imagery. Phases 6 (1899/1904 CE; RG) and 7 (1912/1917 CE; RG) were dated via lichenometry, although no independent evidence is available to corroborate these estimates. For positions 8–10, however, lichenometric ages based on RG thalli are fully consistent with the glacier outlines observed in historical aerial photographs.

Our CRE dating results also reveal discrepancies with both our lichenometry data and older lichenometric estimates (Caseldine 1983, 1985, 1987). For example, Caseldine (1983) recorded thalli exceeding 38 mm in the oldest lichen locality B—located near our Phase 1 outline—within the glaciated area in 1979. In contrast, we found no lichens at that site, likely due to recurrent snow avalanches. Nevertheless, CRE dating indicates that this locality has an exposure age of >2.6±0.5 ka ($n = 2$). Caseldine & Cullingford (1981) also noted the absence of large lichens on or beyond the outermost moraines. In younger moraines (late 19th century), however, lichen sizes correspond well to relative moraine ages.

The limited reliability of lichenometry for phases 1–5 may stem from methodological limitations in Iceland for surfaces older than 120–200 years, due to thallus coalescence, interspecies competition and a reduced growth rate beyond the linear phase (Maizels & Dugmore 1985; Thompson & Jones 1986; Evans *et al*. 1999). Moreover, the former glacier area is frequently impacted by snow avalanches, with snow remnants persisting on the valley floor well into summer. These events can devastate lichen populations—sometimes eliminating up to 90% of thalli in affected areas (Benedict 1993; Bidussi *et al*. 2016; Sancho *et al*. 2017). Consequently, it is unlikely that the oldest lichens survive indefinitely in this environment (Osborn *et al*. 2015). As a result, lichen recolonization may occur repeatedly, leading to ages that underestimate the true timing of deglaciation for phases 1–5.

In contrast, surfaces deglaciated over the past 100–120 years (i.e. within ice-marginal positions 6–12) offer a greater likelihood of preserving original lichen populations. This is supported by thalli whose ages match the deglaciation dates inferred from historical imagery (lichen localities GLJUF-10, -11, -12 and -13).

The evolution of Gljúfurárjökull in the context of other glaciers in Tröllaskagi

The results of this study suggest that the outermost moraines (phases 1 and 2), previously attributed to the late 19th century (Caseldine 1983, 1985, 1987), are significantly older—potentially exceeding 2.6±0.5 ka ($n = 2$). In contrast, the samples considered outliers (9.7±0.9 and 8.5±0.8 ka) may have been reworked from older Preboreal moraines during subsequent Neoglacial advances. Boulders of similar age have been identified using CRE in other valleys across Tröllaskagi. For instance, in the Fremri-Grjótárdalur cirque (17 km to the west, in VíÞinesdalur valley; Fernández-Fernández *et al*. 2020), push moraines formed by debris-free glaciers yielded a mean exposure age of 10.8±1.0 ka ($n = 2$), while deposits from a collapsed glacier front—likely related to debris-covered or rock glaciers—had a mean exposure age of 9.4±1.0 ka ($n = 2$). A similar situation is observed in the Hofsdalur valley (17 km to the west), where push moraines in north-facing cirques show exposure ages of 9.8±1.0 ka ($n = 4$), 9.2±1.0 ka ($n = 3$) and 12.5±1.3 ka ($n = 1$) (Tanarro *et al*. 2021). Additionally, the former terminus of a collapsed debris-covered glacier in the same valley yielded a mean age of 10.1±1.1 ka ($n = 2$). Supporting this, a moraine in Þverárdalur has been interpreted as older than 9 ka based on tephrochronology (Wastl & Stötter 2005).

In consequence, although Preboreal-age moraines have not been definitively identified at Gljúfurárjökull, the evidence from across Tröllaskagi suggests that such early Preboreal features are not uncommon and should be considered.

Glacial Phase 2 yields a CRE age of 2.6±0.5 ka ($n = 2$), Phase 3: 3.2±1.1 ka ($n = 7$) and Phase 4: 2.5±0.2 ka ($n = 2$). Despite the relatively large sample set, these results only confirm that these moraines are at least 2.5 ka in age. They are, therefore, interpreted as marking glacier advances or standstills during the Neoglacial period.

Neoglacial moraines are widespread throughout Tröllaskagi. At the Tungnahryggsjökull glaciers—located in the Vesturdalur and Austurdalur valleys (10 and 8 km west, respectively)—the oldest dated moraines yield calibrated radiocarbon ages of 1.3±0.2 and 1.6±0.2 cal. ka BP ($n = 2$), although older undated moraines are present (Fernández-Fernández *et al*. 2019). In HéÞinsdalur valley, a collapsed debris-covered glacier terminus has a mean CRE age of 2.4±0.3 ka ($n = 3$). Due to the insulating effects of debris, the stabilization of this front likely postdates the actual glacier advance (Palacios *et al*. 2021). Radiocarbon-dated moraines in Vatnsdalur and Bægisárdalur—approximately 12 km from Gljúfurárjökull—yield minimum ages of 4.7±0.2 and 4.2±0.6 cal. ka BP, respectively, and are interpreted as among the earliest Neoglacial advances in the region (Häberle 1991; Stötter 1991; Stötter *et al*. 1999). Although no moraines of this age have yet been CRE-dated in Tröllaskagi, a moraine in Barkárdalur was dated by radiocarbon (wood and soil beneath the moraine) to 2.2±0.1 cal. ka BP (Häberle 1991; Stötter *et al*. 1999).

Glacial Phase 5 presents CRE ages ranging from 2.1 ka to several hundred years in the most distal sectors.

This may correspond to Phase 2 in the Tungnahryggsjökull glaciers (1.3±0.2 and 1.6±0.2 cal. ka BP; $n = 2$). Similarly, aged moraines are present in Barkárdalur valley, where radiocarbon dating of a buried soil yielded 1.5±0.9 cal. ka BP (Häberle 1991; Stötter *et al.* 1999).

Glacial Phases 6 (1904–1899 CE) and 7 (1917/1912 CE) correspond to documented LIA advances, dated by lichenometry and corroborated by historical sources describing two significant glacier advances in Iceland, with some representing the LIA maximum (Eyþórsson 1935; Caseldine & Stötter 1993; AÞalgeirsdóttir *et al.* 2020; Hannesdóttir *et al.* 2020). At this time, the glacier front stood ∼800 m behind the maximum position (Phase 1) and ∼65 m higher in elevation. The ELA, derived via the AAR method, was 44 m higher during Glacial Phase 6 (likely the LIA maximum) than during Glacial Phase 1 (>2.6±0.5 ka), which had previously been interpreted as the LIA maximum.

A comparison of phases 4 (2.5±0.2 ka), 6 (1904–1899 CE) and 7 (∼1917 CE) of Gljúfurárjökull with similar phases in three other glaciers studied with the same methodology (Tungnahryggsjökull W and E, and HéÞinsjökull; Table 8) shows that Gljúfurárjökull consistently maintains a lower ELA—about 130 m lower—and a glacier front located ∼100 m lower than the others. Gljúfurárjökull also shows a progressive ELA rise during the 20th and 21st centuries. Between 1904–1899 CE (Phase 6) and 1946 CE (Ice-Marginal Position 8), the ELA rose by 13 m and by 25 m by 2005 CE. These increases are about half the values previously estimated for this glacier (Caseldine & Stötter 1993), reflecting a reassessment of glacier extent that places the former maximum 800 m further than previously thought. As a result, the summer temperature depression during the LIA maximum may be revised from −2 °C (Caseldine & Stötter 1993) to around −1 °C. ELA-derived temperature reductions from the Phase 1 maximum are even smaller, estimated at −0.2/0.3 °C to −0.5 °C. These values should be interpreted cautiously, however, due to the specific conditions of Tröllaskagi's cirque glaciers, including enhanced snow accumulation from plateau wind drift and avalanches (Caseldine & Stötter 1993; Stötter *et al.* 1999; Fernández-Fernández *et al.* 2017; Brynjólfsson 2019, 2020, 2021).

Since 1946 CE, ice-marginal positions based on the earliest aerial photographs of Gljúfurárjökull have been supplemented with data from the Icelandic Glaciological Society's Jöklavefsjá (Glacier Portal for Iceland; https://islenskirjoklar.is) and previous observations by Eyþórsson (1963). Other authors have also documented these changes (Fernández-Fernández *et al.* 2017; Brito *et al.* 2023; Tables 9, 10; Figs 10, 11). Regarding glacier area evolution (Table 9, Fig. 10), our findings indicate a similar pattern of retreat from 1946 CE onwards compared to earlier studies, although absolute values are lower—up to 300 km^2 less—likely due to improved accuracy from modern digital models. The magnitude of glacier front retreat between specific time intervals is also comparable, typically differing by about 30 m (Table 10, Fig. 11). The use of GPS data to refine digital elevation model assessments likely contributes to the increased precision of our results.

Comparative analysis of the post-LIA evolution of the four debris-free glaciers (Gljúfurárjökull, Tungnahryggsjökull W and E, and HéÞinsjökull), all studied using the same methodology, reveals divergent trends in maximum extent, glacier front altitude and ELA rise. These differences highlight the influence of localized climatic conditions and glacier characteristics on the behaviour in small glacial cirques (Table 8).

The evolution of Gljúfurárjökull in the context of Iceland and the Arctic

Gljúfurárjökull during the Early Holocene (11.7–8.2 ka). – Moraines from Preboreal advances are documented across Iceland. At the onset of the Holocene (∼11.7 ka), Icelandic glaciers experienced a major retreat, with glacier termini receding beyond the present coastline in fjord regions (Pétursson *et al.* 2015; Benediktsson *et al.* 2024). This retreat corresponds to the warming detected in Greenland ice-core records (Rasmussen *et al.* 2014).

Shortly thereafter, glaciers readvanced during the Preboreal (11.3–11.1 ka) over much of Iceland, in many cases reaching limits similar to those of the Younger Dryas (Benediktsson *et al.* 2024). For instance, the prominent BúÞi moraines in Iceland's interior exhibit a polygenetic origin, with outer segments formed during the Younger Dryas and inner parts during the Preboreal advance (NorÞdahl *et al.* 2008; Pétursson *et al.* 2015; Benediktsson *et al.* 2024). Similar polygenetic moraine systems have been observed in western Iceland (Sigfúsdóttir *et al.* 2018; Sigfúsdóttir & Benediktsson 2020).

While central Iceland's ice caps expanded substantially during the Preboreal, this contrasts with the limited advance observed in cirques within Tröllaskagi (as discussed previously). In fact, outlet glaciers from the central ice caps advanced sufficiently to reach SkagafjörÞur and EyjafjörÞur—fjords flanking Tröllaskagi to the west and east, respectively (Ingólfsson *et al.* 1997; NorÞdahl & Einarsson 2001; NorÞdahl & Pétursson 2005; Pétursson *et al.* 2015; Andrés *et al.* 2019).

A similar Early Holocene glacial history is seen in Scandinavia, where Preboreal moraines lie close to those of the Younger Dryas (Lane *et al.* 2020; Nesje & Matthews 2024), correlating with cold episodes observed in Greenland ice cores at ∼10.9 ka and ∼10.2 ka (Vinther *et al.* 2006). Some of the youngest Preboreal moraines are located no more than ∼1 km from LIA moraines (Dahl *et al.* 2002). Comparable Early Holocene advances are documented in remnants of the Laur-

Table 8. Comparison of the evolution of the glacial dimensions and ELA on Gljúfurárjökull, according to the data obtained in this work for each stage. This data can be contrasted with the evolution of the glacial dimensions and ELA of glaciers where similar methods have been applied: western and eastern Tungnahryggsjökull (Fernández-Fernández *et al.* 2019) and HéÞinsjökull (Palacios *et al.* 2021).

Gljúfurárjökull						Western Tungnahryggsjökull				Eastern Tungnahryggsjökull				HéÞinsdalsjökull			
Glacial Phase/Ice terminal position (TP)	Inferred ages	Length (m)	Area (km^2)	Min. elev. (m a.s.l.)	ELA AAR (m a.s.l.)	Length (m)	Area (km^2)	Min. elev. (m a.s.l.)	ELA AAR (m a.s.l.)	Length (m)	Area (km^2)	Min. elev. (m a.s.l.)	ELA AAR (m a.s.l.)	Length (m)	Area (km^2)	Min. elev. (m a.s.l.)	ELA AAR (m a.s.l.)
Phase 1	>2.6±0.5 ka	4145	3.939	485	914												
Phase 2	2.6±0.5 ka	4025	3.886	495	924												
Phase 3	3.2±1.1 ka	3938	3.831	503	927												
Phase 4	2.5±0.2 ka	3773	3.639	513	947									5150	6.98	610	1042
Phase 5	From 2.1 ka to a few hundred years	3615	3.565	525	954	5483	8.87	547	1047	3733	5.26	631	1032				
Phase 6	1899/ 1904 CE	3433	3.499	543	958	3601	6.98	768	1094	2911	4.71	722	1055	4440	6.04	683	1059
Phase 7	1912/ 1917 CE	3334	3.440	550	964	3452	6.94	785	1094	2755	4.56	735	1061				
TP 8	1946 CE	3280	3.403	556	971	3406	6.91	796	1094	2722	4.54	742	1060	3290	5.15	934	1085
TP 9	1960 CE	3126	3.344	573	973												
TP 10	1985 CE	3010	3.271	587	982	3338	6.67	806	1100	2477	4.02	774	1061				
TP 11	1994 CE	3030	3.277	585	980	3311	6.68	810	1102								
TP 12	2000 CE	3006	3.256	589	979	3203	6.57	830	1098	2513	4.02	763	1061	3270	4.92		1095
TP 13	2005 CE	2927	3.209	598	983	3183	6.47	834	1099	2485	3.88	767	1065				
TP 14	2016 CE	2802	3.164	613	992												
TP 15	2017 CE	2799	3.108	614	988												
TP 16	2019 CE	2788	3.089	618	992									3240	4.67	972	1104

Table 9. Evolution of glacier area (km^2) interpreted by different sources (Jöklavefsja, Glacier Portal for Iceland; https://islenskirjoklar.is/#) (Fernández-Fernández *et al.* 2017; Brito *et al.* 2023), compared to the results of this work.

Year	Jöklavefsja	Fernández-Fernández *et al.* (2017)	Brito *et al.* (2023)	Present work
1890	3.950			
1946		3.540	3.630	3.403
1960				3.344
1985		3.407	3.560	3.271
1994		3.413	3.570	3.277
2000	3.259	3.384		3.256
2005		3.335		3.209
2014	3.301			
2016			3.380	3.164
2017	3.218			3.108
2019	3.218		3.360	3.089

entide Ice Sheet and the Greenland Ice Sheet (Young *et al.* 2020). In both North America and Greenland, glacial advances corresponding to the 9.2 and 8.2 ka events have been recognized, which align with cold spells identified in Greenland ice-core records (Rasmussen *et al.* 2007) and North Atlantic marine sediments (Jennings *et al.* 2015).

In Iceland, following the Preboreal advance, glaciers retreated rapidly, reaching extents similar to those of the 20th century in less than a millennium (Pétursson *et al.* 2015; Andrés *et al.* 2019). This rapid retreat is evidenced by the widespread distribution of the Saksunarvatn tephra (~10.3 cal. ka BP) around modern glacier margins (Óladóttir *et al.* 2020). A glacial advance related to the 9.2 ka event has been documented at LeirufjörÞur (Drangajökull; Brynjólfsson *et al.* 2015). However, moraines associated with the 8.2 ka event have not been identified in Iceland to date (Pétursson *et al.* 2015; Benediktsson *et al.* 2024).

Gljúfurárjökull in the context of Middle Holocene (8.2–4.2 ka). – According to our results, Gljúfurárjökull did not experience any glacial advance during the Middle Holocene. After the Preboreal, Icelandic glaciers retreated behind their present-day ice-marginal positions and may have even disappeared entirely between 8.0 and at least 6.5 cal. ka BP (Geirsdóttir *et al.* 2009; Ingólfsson *et al.* 2010; Geirsdóttir 2011; Anderson

Table 10. Retreat in metres of the glacier snout, compared to its position in 1939 and 1946 (first aerial photo of the glacier) in different years interpreted by different sources (Jöklavefsja, Glacier Portal for Iceland; https://islenskirjoklar.is/#; Eyþórsson 1963; Fernández-Fernández *et al.* 2017; Brito *et al.* 2023) compared to the results of this work.

Year	Eyþórsson (1963)	Jöklavefsja	Fernández-Fernández *et al.* (2017)	Brito *et al.* (2023)	Present work
1939	0	0			
1946			0	0	0
1953	−46	−46			
1955	−114	−114			
1956	−139	−139			
1957	−155	−162			
1958	−161	−168			
1959	−182	−189			
1960	−197				−154
1962		−234			
1964		−271			
1966		−287			
1969		−317			
1970		−312			
1971		−323			
1972		−339			
1976		−413			
1978		−402			
1979		−363			
1981		−333			
1983		−308			
1984		−313			
1985		−300	−275	−276.4	−270
1994		−263	−255	−251.4	−250
2000		−284	−281		−274
2004		−304			
2005			−358	−350.5	−353
2015		−421			
2016				−464	−478
2017		−463			
2019		−477		−492	−492

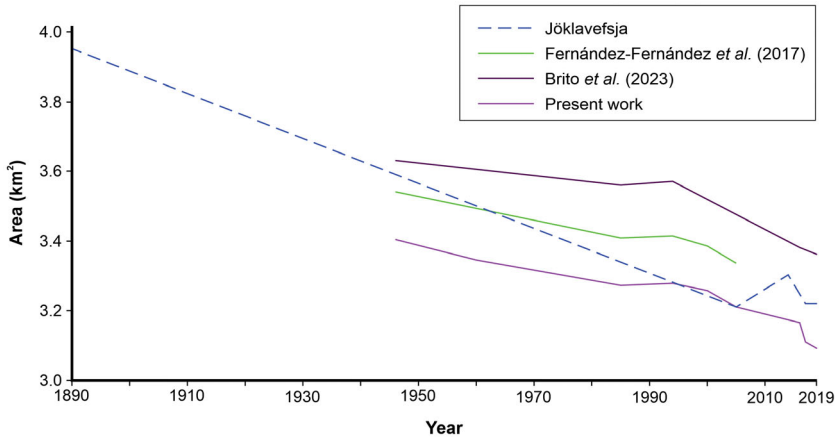

Fig. 10. Glacier snout retreat of Gljúfurárjökull (m) from 1939 (1946) to 2019, according to the different sources of analysis (see Table 9).

et al. 2019). However, multiple horizons of distally deposited, ocean-rafted pumice dated to the Middle Holocene have been interpreted as evidence of jökulhlaups triggered by subglacial eruptions beneath a persistent Mýrdalsjökull ice cap (Farnsworth *et al.* 2020b).

This pattern is comparable to other regions. In Scandinavia, most glaciers disappeared following the 8.2 ka event or were reduced to a size much smaller than today (Nesje & Matthews 2024). In Svalbard, glaciers reached their minimum Holocene extent—smaller than at present—between 8.0 and 6.0 ka, and some may have vanished entirely (Farnsworth *et al.* 2020a; Farnsworth & Allaart 2024). Nevertheless, it is assumed that glaciers persisted at higher elevations in northern and eastern Svalbard during the Holocene Thermal Maximum (Farnsworth *et al.* 2024). In Franz Josef Land, glaciers had already been significantly reduced and remained smaller than present since around 11 ka (Solomina *et al.* 2024).

The Greenland Ice Sheet had retreated behind its current margins by 10 ka and largely disappeared from southern Greenland during the Middle Holocene (Larsen *et al.* 2015; Pedersen & Christensen 2019; Lesnek *et al.* 2020). Similarly, the Laurentide Ice Sheet collapsed in its offshore sector after 8.2 ka and disappeared entirely between 6.3 and 7.1 ka (Dalton *et al.* 2023).

Gljúfurárjökull glacial advances within the Late Holocene, from 4.2 ka to the end of the LIA. – The main finding of this study is the evidence that Gljúfurárjökull repeatedly advanced and re-advanced during the Neoglacial period or experienced prolonged phases of frontal stagnation, particularly between 3.5 and 2.0 ka, over a more extensive area than during the LIA. This correlates with the

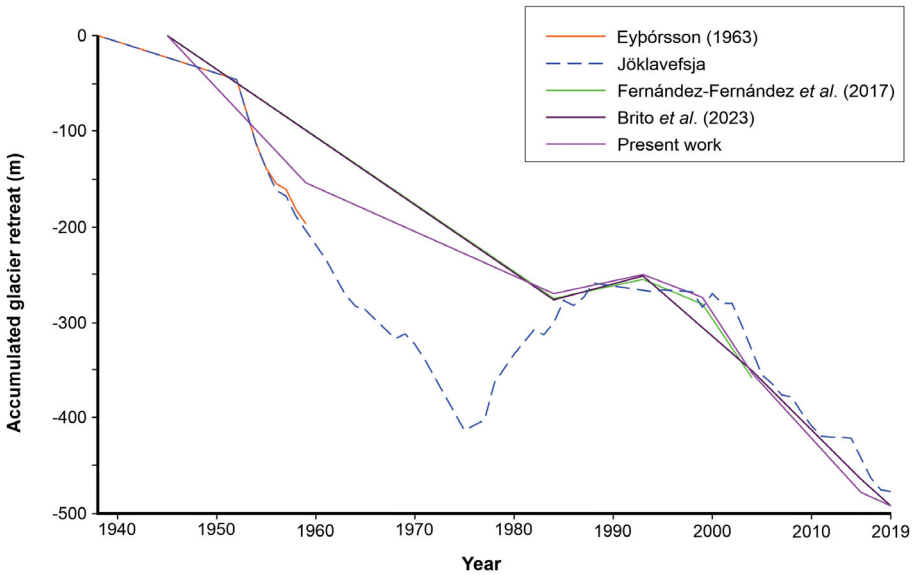

Fig. 11. Glacier area retreat of Gljúfurárjökull (km^2) from 1890 (1946) to 2019, according to the different sources of analysis (see Table 10).

reformation of the Langjökull and Vatnajökull ice caps around 5.5 and 4.4 cal. ka BP (Larsen *et al*. 2012; Striberger *et al*. 2012). However, the timing of the maximum Late Holocene extent varies among glaciers (Pétursson *et al*. 2015; Benediktsson *et al*. 2024).

In Scandinavia, numerous pieces of evidence have been found of glacial advances, mainly from ∼4.5 cal. ka BP (Carrivick *et al*. 2022; Nesje & Matthews 2024). In Svalbard, new findings are emerging of various glaciers peaking after 2 ka (Farnsworth & Allaart 2024). In the Polar Urals, the glaciers were reconstructed from ∼4.0 ka. In Novaya Zemlya and Franz Josef Land, only the LIA advance is known as the maximum in the Late Holocene (Solomina *et al*. 2024). The Greenland Ice Sheet advanced in the Late Holocene but with many regional differences (Briner *et al*. 2016). In some sectors, it reached its minimum extent at ∼4 ka, even as late as 2 ka for some regions and afterwards advanced (Young & Briner 2015).

Knowledge in the Arctic about the extent of glacial advances during the Late Holocene is limited. As previously noted, in most regions the LIA seems to be given more prominence, although, as in Iceland, earlier major advances are being discovered as research progresses. The Phases 3 (3.2±1.1 ka), 4 (2.5±0.2 ka) and 5 (between 2.1 ka and a few hundred years) of Gljúfurárjökull are, however, paralleled by the much more detailed information available from the Alps, where glaciers reached maximum extents at ∼4.2, 3.5, 2.8 to 2.6, 2.1, 1.4 and 1.15 ka and where many moraines previously considered to be from the LIA have been shown to predate it (Le Roy *et al*. 2024).

Gljúfurárjökull glacial retreat from the end of the LIA to the present. – As observed at Gljúfurárjökull, the large ice caps of Iceland began retreating in the early 20th century—a trend that has continued to the present day, interrupted only by brief periods of stagnation or minor advances. The most notable post-LIA advance occurred during the 1990s (AÞalgeirsdóttir *et al*. 2020; Hannesdóttir *et al*. 2020). At Gljúfurárjökull, this advance is evidenced by Ice-Marginal Position 11 (1994) overtopping position 10 (1985). A similar pattern of glacier behaviour has been observed in Scandinavia, where the most significant post-LIA advance also took place during the 1980s–1990s CE (Nesje & Matthews 2024).

Conclusions

Gljúfurárjökull is one of the most thoroughly studied valley glaciers in Iceland. The results of this study are as follows:

- Gljúfurárjökull has followed an evolutionary trajectory similar to other valley glaciers and ice cap outlets in Iceland.
- We reconstruct the valley glacier's Holocene glacier history by CRE dating boulders deposited on a series of polygenic moraines. Results suggest the moraines have been reworked during multiple Late Holocene glacial advances during the Neoglacial period. This chronology aligns with those established for most other Icelandic glaciers.
- We find no evidence of a Preboreal readvance from Gljúfurárjökull. The Early Holocene was likely followed by a prolonged period of minimal glacial activity until the onset of Neoglacial advances.
- During the Late Holocene, the glacier experienced several oscillations culminating in the LIA advances.
- Contrary to earlier interpretations of Gljúfurárjökull's history, our results suggest that the LIA advance was not the most extensive Late Holocene positioning of the ice margin. In fact, some earlier Neoglacial advances—particularly those occurring around 2.5 ka—were more extensive than the LIA advance.
- The oldest moraine ages derived from lichenometry are inconsistent both among themselves and with the CRE data. We infer that these ages reflect the timing of the most recent post-glacial disturbance rather than the original stabilization of the moraines.
- For the youngest moraines (less than 130 years old), the lichenometric ages appear reliable, supported by internal consistency and correspondence with historical aerial imagery of glacier extent.
- Since the end of the LIA in the early 20th century, Gljúfurárjökull has retreated; however, we identified notable local variations in equilibrium line altitude, even between neighbouring glaciers studied using the same methods.
- The only period of glacier re-advance during the 20th century occurred in the 1980s and 1990s, coinciding with the most widespread advance recorded across the Arctic.

Acknowledgements. – This research was framed within the NEOICE project: 'Reconstruction of Neoglacial oscillations in Iceland', ref. PID2020-113798GB-C32, funded by MCIN/AEI/10.13039/5011 00011033. The ^{36}Cl measurements were performed at the ASTER AMS National Facility (CEREGE, Aix-en-Provence), supported by the INSU/CNRS and the ANR through the 'Projets thématiques d'excellence' programme for the 'Équipements d'excellence' ASTER-CEREGE action and the IRD. We thank the GFAM team (Physical Geography of High Mountains and Polar Areas) research group of the Complutense University for its research support, Ángeles Salas Aizpuru for her work on the samples in the laboratory of the Complutense University of Madrid and Manuel Rodríguez Mena, for his work on the samples in the laboratory of CEREGE. We would like to thank three anonymous reviewers for their very constructive comments. Special thanks to Ívar Örn Benediktsson, for his valuable comments on the revision of the manuscript, as well as the editor Jan A. Piotrowski, who greatly contributed to improve an earlier draft of the manuscript. The authors declare that they have no known competing financial interests or personal relationships that could have appeared to influence the work reported in this paper.

Author contributions. – NA: coordination of all phases of the research and writing of a first draft of the manuscript, conception and design, analysis and interpretation of data, leading the fieldwork, geomorpho-

logical analysis, sampling and data processing. JMF-F: Fieldwork, geomorphological analysis, glacier reconstruction, equilibrium-line altitude calculations, laboratory tasks (sample processing, exposure age calculations), discussion of the results, contribution to the geomorphological mapping and writing. DP: Conception and design, or analysis and interpretation of the data, fieldwork, geomorphological analysis, discussion of the results, contribution to the geomorphological mapping and writing. IS: Supervision of the whole process of the sample strategy and processing and interpretation of the results. Thorough correction of the manuscript. LGS: Fieldwork, lichenometric analysis, discussion of the results. SB: Fieldwork, discussion of the results and contribution to the writing. ÞS: Discussion of the results and contribution to the writing. WRF: Discussion of the results and contribution to the writing. LMT: Fieldwork, discussion of the results and contribution to the writing. MB: Data analysis, discussion of the results and contribution to the writing. JSG: Data analysis, discussion of the results and contribution to the writing. RBG-G: Data analysis, discussion of the results and contribution to the writing. ASTER Team: AMS measurements of the ^{36}Cl samples.

Data availability statement. – The data that support the findings of this study are available from the corresponding author upon reasonable request.

References

AÞalgeirsdóttir, G., Magnússon, E., Pálsson, F., Thorsteinsson, T., Belart, J. M. C., Jóhannesson, T., Hannesdóttir, H., SigurÞsson, O., Gunnarsson, A., Einarsson, B., Berthier, E., Schmidt, L. S., Haraldsson, H. H. & Björnsson, H. 2020: Glacier changes in Iceland from ∼1890 to 2019. *Frontiers in Earth Science 8*, 523646. https://doi.org/10.3389/feart.2020.523646.

Anderson, L. S., Geirsdóttir, Á., Flowers, G. E., Wickert, A. D., AÞalgeirsdóttir, G. & Thorsteinnsson, T. 2019: Controls on the lifespan of Icelandic ice caps. *Earth and Planetary Science Letters 527*, 115780. https://doi.org/10.1016/j.epsl.2019.115780.

Andrés, N., Palacios, D., Sæmundsson, Þ., Brynjolfsson, S. & Fernández-Fernández, J. M. 2019: The rapid deglaciation of the SkagafjorÞur fjord, northern Iceland. *Boreas 48*, 92–106. https://doi.org/10.1111/bor.12341.

Applegate, P. J., Urban, N. M., Laabs, B. J. C., Keller, K. & Alley, R. B. 2010: Modeling the statistical distributions of cosmogenic exposure dates from moraines. *Geoscientific Model Development 3*, 293–307. https://doi.org/10.5194/gmd-3-293-2010.

Balco, G. 2020: Glacier change and paleoclimate applications of cosmogenic-nuclide exposure dating. *Annual Review of Earth and Planetary Sciences 48*, 21–48. https://doi.org/10.1146/annurev-earth-081619-052609.

Balco, G., Stone, J., Lifton, N. & Dunai, T. 2008: A complete and easily accessible means of calculating surface exposure ages or erosion rates from ^{10}Be and ^{26}Al measurements. *Quaternary Geochronology 3*, 174–195. https://doi.org/10.1016/j.quageo.2007.12.001.

Benedict, J. B. 1993: A 2000-year lichen-snowkill chronology for the Colorado Front Range, USA. *The Holocene 3*, 27–33. https://doi.org/10.1177/095968369300300103.

Benediktsson, Í. Ö., Brynjólfsson, S., Ásbjörnsdóttir, L. & Farnsworth, W. R. 2024: Holocene glacial history and landforms of Iceland. *In* Palacios, D., Hughes, P., Jomelli, V. & Tanarro, L. M. (eds.): *European Glacial Landscapes*, 193–224. Elsevier, Amsterdam. https://doi.org/10.1016/B978-0-323-99712-6.00012-X.

Benn, D. I. & Hulton, N. R. J. 2010: An ExcelTM spreadsheet program for reconstructing the surface profile of former mountain glaciers and ice caps. *Computers & Geosciences 36*, 605–610. https://doi.org/10.1016/j.cageo.2009.09.016.

Bidussi, M., Solhaug, K. A. & Gauslaa, Y. 2016: Increased snow accumulation reduces survival and growth in dominant mat-forming arctic-alpine lichens. *The Lichenologist 48*, 237–247. https://doi.org/10.1017/S0024282916000086.

Bradwell, T. 2010: Studies on the growth of Rhizocarpon geographicum in NW Scotland, and some implications for lichenometry. *Geografiska Annaler: Series A, Physical Geography 92*, 41–52. https://doi.org/10.1111/j.1468-0459.2010.00376.x.

Braucher, R., Keddadouche, K., Aumaître, G., Bourlès, D. L., Arnold, M., Pivot, S., Baroni, M., Scharf, A., Rugel, G. & Bard, E. 2018: Chlorine measurements at the 5MV French AMS national facility ASTER: associated external uncertainties and comparability with the 6MV DREAMS facility. *Nuclear Instruments and Methods in Physics Research Section B: Beam Interactions with Materials and Atoms 420*, 40–45. https://doi.org/10.1016/j.nimb.2018.01.025.

Briner, J. P., Kaufman, D. S., Manley, W. F., Finkel, R. C. & Caffee, M. W. 2005: Cosmogenic exposure dating of late Pleistocene moraine stabilization in Alaska. *Geological Society of America Bulletin 117*, 1108–1120. https://doi.org/10.1130/B25649.1.

Briner, J. P., McKay, N. P., Axford, Y., Bennike, O., Bradley, R. S., de Vernal, A., Fisher, D., Francus, P., Fréchette, B., Gajewski, K., Jennings, A., Kaufman, D. S., Miller, G., Rouston, C. & Wagner, B. 2016: Holocene climate change in Arctic Canada and Greenland. *Quaternary Science Reviews 147*, 340–364. https://doi.org/10.1016/j.quascirev.2016.02.010.

Brito, M., Andrés, N., Fernández-Fernández, J. M., Tanarro, L. M., Brynjólfsson, S. & Sæmundsson, Þ. 2023: *Analysing the response of debris-free glaciers in Tröllaskagi (northern Iceland) to recent warming through differential interferometry and other remote sensing techniques.* PalaeoArc 2023, Akureyri, Iceland. August 27th–30th 2023.

Brynjólfsson, S. 2019: *Afkoma jökla á Tröllaskaga jökulárið 2017–2018*. NÍ-19004 Report. NáttúrufræÞistofnun Islands ISSN 1670-0120, 24 pp. Akureyri, Iceland.

Brynjólfsson, S. 2020: *Afkoma jökla á Tröllaskaga jökulárið 2018–2019*. NÍ-20005 Report. NáttúrufræÞistofnun Islands ISSN 1670-0120, 23 pp. Akureyri, Iceland.

Brynjólfsson, S. 2021: *Afkoma jökla á Tröllaskaga jökulárið 2019–2020*. NÍ-21003 Report. NáttúrufræÞistofnun Islands ISSN 1670-0120, 24 pp. Akureyri, Iceland.

Brynjólfsson, S., Schomacker, A., Ingólfsson, O. & Keiding, J. K. 2015: Cosmogenic ^{36}Cl exposure ages reveal a 9.3 ka BP glacier advance and the Late Weichselian-Early Holocene glacial history of the Drangajökull region, northwest Iceland. *Quaternary Science Reviews 126*, 140–157. https://doi.org/10.1016/j.quascirev.2015.09.001.

Carrivick, J. L., Andreassen, L. M., Nesje, A. & Yde, J. C. 2022: A reconstruction of Jostedalsbreen during the Little Ice Age and geometric changes to outlet glaciers since then. *Quaternary Science Reviews 284*, 107501. https://doi.org/10.1016/j.quascirev.2022.107501.

Caseldine, C. J. 1983: Resurvey of the margins of Gljúfurárjökull and the chronology of recent deglaciation. *Jökull 33*, 111–118. https://doi.org/10.33799/jokull1983.33.111.

Caseldine, C. J. 1985: The extent of some glaciers in northern Iceland during the Little Ice Age and the nature of recent deglaciation. *The Geographical Journal 151*, 215–227. https://doi.org/10.2307/633535.

Caseldine, C. J. 1987: Neoglacial glacier variations in northern Iceland: examples from the EyjafjörÞur area. *Arctic and Alpine Research 19*, 296–304. https://doi.org/10.1080/00040851.1987.12002604.

Caseldine, C. 1991: Lichenometric dating, lichen population studies and Holocene glacial history in Tröllaskagi, Northern Iceland. *In* Maizels, J. K. & Caseldine, C. (eds.): *Environmental Change in Iceland: Past and Present*, 219–233. Springer, Dordrecht. https://doi.org/10.1007/978-94-011-3150-6_15.

Caseldine, C. J. & Cullingford, R. A. 1981: Recent mapping of Gljúfurárjokull and Gljúfurárdalur. *Jökull 31*, 11–22. https://doi.org/10.33799/jokull1981.31.011.

Caseldine, C. & Hatton, J. 1994: Interpretation of Holocene change for the Eyajafjördur area of Northern Iceland from pollen-analytical data. *In* Stötter, J. & Wilhelm, F. (eds.): *Environmental Change in Iceland. Münchener Geografische Abhandlungen. R. B Bd. B* 12, 41–62. Springer, Netherlands.

Caseldine, C. J. & Stötter, J. 1993: "Little Ice Age" glaciation of Tröllaskagi peninsula, northern Iceland: climatic implications for reconstructed equilibrium line altitudes (ELAs). *The Holocene 3*, 357–366. https://doi.org/10.1177/095968369300300408.

Dahl, S. O., Nesje, A., Lie, Ä., Fjordheim, K. & Matthews, J. A. 2002: Timing, equilibrium-line altitudes and climatic implications of two

early Holocene glacier readvances during the Erdalen event at Jostedalsbreen, western Norway. *The Holocene 12*, 17–25. https://doi.org/10.1191/0959683602hl516rp.

Dalton, A. S., Dulfer, H. E., Margold, M., Heyman, J., Clague, J. J., Froese, D. G., Gauthier, M. S., Hughes, A. L. C., Jennings, C. E., Norris, S. L. & Stoker, B. J. 2023: Deglaciation of the north American ice sheet complex in calendar years based on a comprehensive database of chronological data: NADI-1. *Quaternary Science Reviews 321*, 108345. https://doi.org/10.1016/j.quascirev.2023.108345.

Dickson, R. R., Lamb, H. H., Malmberg, S. A. & Colebrook, J. M. 1975: Climatic reversal in northern North Atlantic. *Nature 256*, 479–482. https://doi.org/10.1038/256479a0.

Dickson, R. R., Meincke, J., Malmberg, S. A. & Lee, A. J. 1988: The "great salinity anomaly" in the Northern North Atlantic 1968–1982. *Progress in Oceanography 20*, 103–151. https://doi.org/10.1016/0079-6611(88)90049-3.

Dugmore, A. J. 1989: Tephrochronological studies of Holocene glacier fluctuations in South Iceland. *In* Oerlemans, J. (ed.): *Glacier Fluctuations and Climatic Change*, 37–55. Springer, Dordrecht. https://doi.org/10.1007/978-94-015-7823-3_3.

Dugmore, A. J. & Sugden, D. E. 1991: Do the anomalous fluctuations of Sólheimajökull reflect ice-divide migration? *Boreas 20*, 105–113. https://doi.org/10.1111/j.1502-3885.1991.tb00299.x.

Evans, D. J. A., Archer, S. & Wilson, D. J. H. 1999: A comparison of the lichenometric and Schmidt hammer dating techniques based on data from the proglacial areas of some Icelandic glaciers. *Quaternary Science Reviews 18*, 13–41. https://doi.org/10.1016/S0277-3791(98)00098-5.

Eyþórsson, J. 1935: On the variations of glaciers in Iceland: some studies made in 1931. *Geografiska Annaler 17*, 121–137. https://doi.org/10.1080/20014422.1935.11880594.

Eyþórsson, J. 1963: Variations of Iceland glaciers 1931–1960. *Jökull 13*, 31–33.

Farnsworth, W. R. & Allaart, L. 2024: Holocene glacial landscapes of Svalbard. *In* Palacios, D., Hughes, P., Jomelli, V. & Tanarro, L. M. (eds.): *European Glacial Landscapes*, 171–191. Elsevier, Amsterdam. https://doi.org/10.1016/B978-0-323-99712-6.00014-3.

Farnsworth, W. R., Allaart, L., Ingolfsson, O., Alexanderson, H., Forwick, M., Noormets, R., Retelle, M. & Schomacker, A. 2020a: Holocene glacial history of Svalbard – status, perspectives and challenges. *Earth-Science Reviews 208*, 103249. https://doi.org/10.1016/j.earscirev.2020.103249.

Farnsworth, W. R., Blake, W., Jr., Guþmundsdóttir, E. R., Ingólfsson, Ó., Kalliokoski, M. H., Larsen, G., Newton, A. J., Óladóttir, B. A. & Schomacker, A. 2020b: Ocean-rafted pumice constrains postglacial relative sea-level and supports Holocene ice cap survival. *Quaternary Science Reviews 250*, 106654. https://doi.org/10.1016/j.quascirev.2020.106654.

Farnsworth, W. R., Ingólfsson, Ó., Brynjólfsson, S., Allaart, L., Kjellman, S. E., Kjær, K. H., Larsen, N. K., Macias-Fauria, M., Siggaard-Andersen, M.-L. & Schomacker, A. 2024: Persistence of Holocene ice cap in northeast Svalbard aided by glacio-isostatic rebound. *Quaternary Science Reviews 331*, 108625. https://doi.org/10.1016/j.quascirev.2024.108625.

Fernández-Fernández, J. M., Andrés, N., Sæmundsson, Þ., Brynjólfsson, S. & Palacios, D. 2017: High sensitivity of North Iceland (Tröllaskagi) debris-free glaciers to climatic change from the 'Little Ice Age' to the present. *The Holocene 27*, 1187–1200. https://doi.org/10.1177/0959683616683262.

Fernández-Fernández, J. M., Palacios, D., Andrés, N., Schimmelpfennig, I., Brynjólfsson, S., Sancho, L. G., Zamorano, J. J., Heiðmarsson, S., Sæmundsson, Þ. & ASTER Team 2019: A multi-proxy approach to Late Holocene fluctuations of Tungnahryggsjökull glaciers in the Tröllaskagi peninsula (northern Iceland). *Science of the Total Environment 664*, 499–517. https://doi.org/10.1016/j.scitotenv.2019.01.364.

Fernández-Fernández, J. M., Palacios, D., Andrés, N., Schimmelpfennig, I., Tanarro, L. M., Brynjólfsson, S., López-Acevedo, F. J., Sæmundsson, Þ. & ASTER Team 2020: Constraints on the timing of debris-covered and rock glaciers: an exploratory case study in the Hólar area, northern Iceland. *Geomorphology 361*, 107196. https://doi.org/10.1016/j.geomorph.2020.107196.

Fink, D., Vogt, S. & Hotchkis, M. 2000: Cross-sections for 36Cl from Ti at Ep=35–150 MeV: applications to in-situ exposure dating. *Nuclear Instruments and Methods in Physics Research Section B: Beam Interactions with Materials and Atoms 172*, 861–866. https://doi.org/10.1016/S0168-583X(00)00200-7.

Fisher, T. G., Smith, D. G. & Andrews, J. T. 2002: Preboreal oscillation caused by a glacial Lake Agassiz flood. *Quaternary Science Reviews 21*, 873–878. https://doi.org/10.1016/S0277-3791(01)00148-2.

Geirsdóttir, Á. 2011: Pliocene and Pleistocene glaciations of Iceland: a brief overview of the glacial history. *Developments in Quaternary Sciences 15*, 199–210. https://doi.org/10.1016/B978-0-444-53447-7.00016-7.

Geirsdóttir, A., Miller, G. H., Axford, Y. & Ólafsdóttir, S. 2009: Holocene and latest Pleistocene climate and glacier fluctuations in Iceland. *Quaternary Science Reviews 28*, 2107–2118. https://doi.org/10.1016/j.quascirev.2009.03.013.

Gudmundsson, H. J. 1997: A review of the Holocene environmental history of Iceland. *Quaternary Science Reviews 16*, 81–92. https://doi.org/10.1016/S0277-3791(96)00043-1.

Häberle, T. 1991: Holocene glacial history of the Hörgárdalur area, Tröllaskagi, northern Iceland. *In* Maizels, J. K. & Caseldine, C. (eds.): *Environmental Change in Iceland: Past and Present*, 193–202. Springer, Dordrecht. https://doi.org/10.1007/978-94-011-3150-6_13.

Hannesdóttir, H., Sigurþsson, O., Þrastarson, R. H., Guþmundsson, S., Belart, J. M. C., Pálsson, F., Magnússon, E., Víkingsson, S., Kaldal, I. & Johannesson, T. 2020: A national glacier inventory and variations in glacier extent in Iceland from the Little Ice Age maximum to 2019. *Jökull 12*, 1–34. https://doi.org/10.33799/jokull2020.70.001.

Helama, S., Jones, P. D. & Briffa, K. R. 2017: Dark Ages Cold Period: a literature review and directions for future research. *The Holocene 27*, 1600–1606. https://doi.org/10.1177/0959683617693898.

Heyman, J., Stroeven, A. P., Harbor, J. M. & Caffee, M. W. 2011: Too young or too old: evaluating cosmogenic exposure dating based on an analysis of compiled boulder exposure ages. *Earth and Planetary Science Letters 302*, 71–80. https://doi.org/10.1016/j.epsl.2010.11.040.

Hooker, T. N. & Brown, D. H. 1977: A photographic method for accurately measuring the growth of crustose and foliose saxicolous lichens. *The Lichenologist 9*, 65–75. https://doi.org/10.1017/S0024282977000073.

Ingólfsson, Ó., Björck, S., Hafliþason, H. & Rundgren, M. 1997: Glacial and climatic events in Iceland reflecting regional North Atlantic climatic shifts during the Pleistocene-Holocene transition. *Quaternary Science Reviews 16*, 1135–1144. https://doi.org/10.1016/S0277-3791(97)00007-3.

Ingólfsson, Ó., Norþdahl, H. & Schomacker, A. 2010: Deglaciation and Holocene glacial history of Iceland. *In* Schomacker, A., Krüger, J. & Kjær, K. H. (eds.): *The Mýrdalsjökull Ice Cap, Iceland. Glacial Processes, Sediments and Landforms on an Active Volcano*, 51–68. Elsevier Science, Amsterdam. https://doi.org/10.1016/S1571-0866(09)01304-9.

James, W. H. M. & Carrivick, J. L. 2016: Automated modelling of spatially-distributed glacier ice thickness and volume. *Computers & Geosciences 92*, 90–103. https://doi.org/10.1016/j.cageo.2016.04.007.

Jennings, A., Andrews, J., Pearce, C., Wilson, L. & Ólfasdótttir, S. 2015: Detrital carbonate peaks on the Labrador shelf, a 13–7 ka template for freshwater forcing from the Hudson Strait outlet of the Laurentide Ice Sheet into the subpolar gyre. *Quaternary Science Reviews 107*, 62–80. https://doi.org/10.1016/j.quascirev.2014.10.022.

Jóhannesson, H. & Sæmundsson, K. 1989: *Geological Map of Iceland. 1:500.000*. Bedrock Icelandic Institute of Natural History, Reykjavik.

Kirkbride, M. P. & Dugmore, A. J. 2001: Timing and significance of mid-Holocene glacier advances in northern and central Iceland. *Journal of Quaternary Science 16*, 145–153. https://doi.org/10.1002/jqs.589.

Kirkbride, M. P. & Dugmore, A. J. 2006: Responses of mountain ice caps in central Iceland to Holocene climate change. *Quaternary Science Reviews 25*, 1692–1707. https://doi.org/10.1016/j.quascirev.2005.12.004.

Kirkbride, M. P. & Dugmore, A. J. 2008: Two millennia of glacier advances from southern Iceland dated by tephrochronology. *Quaternary Research 70*, 398–411. https://doi.org/10.1016/j.yqres.2008.07.001.

Koblet, T., Gärtner-Roer, I., Zemp, M., Jansson, P., Thee, P., Haeberli, W. & Holmlund, P. 2010: Reanalysis of multi-temporal aerial images of Storglaciären, Sweden (1959-99); part 1: Determination of length, area, and volume changes. *The Cryosphere 4*, 333–343. https://doi.org/10.5194/tc-4-333-2010.

Kugelmann, O. 1991: Dating recent glacier advances in the SvarfaÞardalur-SkiÞadalur area of northern Iceland by means of a new lichen curve. *In* Maizels, J. K. & Caseldine, C. (eds.): *Environmental Change in Iceland: Past and Present*, 203–217. Springer, Dordrecht. https://doi.org/10.1007/978-94-011-3150-6_14.

Lal, D. 1991: Cosmic ray labeling of erosion surfaces: in situ nuclide production rates and erosion models. *Earth and Planetary Science Letters 104*, 424–439. https://doi.org/10.1016/0012-821X(91)90220-C.

Lane, T. P., Paasche, Ä., Kvisvik, B., Adamson, K. R., Rodés, Á., Patton, H., Gomez, N., Gheorghiu, D., Bakke, J. & Hubbard, A. 2020: Elevation changes of the Fennoscandian Ice Sheet interior during the last deglaciation. *Geophysical Research Letters 47*, e2020GL088796. https://doi.org/10.1029/2020GL088796.

Larsen, N. K., Kjær, K. H., Lecavalier, B., Bjørk, A. A., Colding, S., Huybrechts, P., Jakobsen, K. E., Kjeldsen, K. K., Knudsen, K. L., Odgaard, B. V. & Olsen, J. 2015: The response of the southern Greenland ice sheet to the Holocene thermal maximum. *Geology 43*, 291–294. https://doi.org/10.1130/G36476.1.

Larsen, D. J., Miller, G. H., Geirsdóttir, Á. & Ólafsdóttir, S. 2012: Nonlinear Holocene climate evolution in the North Atlantic: a high-resolution, multi-proxy record of glacier activity and environmental change from Hvítárvatn, central Iceland. *Quaternary Science Reviews 39*, 14–25. https://doi.org/10.1016/j.quascirev.2012.02.006.

Larsen, N. K., Søndergaard, A. S., Levy, L. B., Laursen, C. H., Bjørk, A. A., Kjeldsen, K. K., Funder, S., Strunk, A., Olsen, J. & Kjær, K. H. 2021: Cosmogenic nuclide inheritance in Little Ice Age moraines – a case study from Greenland. *Quaternary Geochronology 65*, 101200. https://doi.org/10.1016/j.quageo.2021.101200.

Le Roy, M., Ivy-Ochs, S., Nicolussi, K., Monegato, G., Reitner, J. M., Colucci, R. R., Ribolini, A., Spagnolo, M. & Stoffel, M. 2024: Holocene glacier variations in the Alps. *In* Palacios, D., Hughes, P. D., Jomelli, V. & Tanarro, L. M. (eds.): *European Glacial Landscapes*, 367–418. Elsevier, Amsterdam. https://doi.org/10.1016/B978-0-323-99712-6.00018-0.

Lesnek, A. J., Briner, J. P., Young, N. E. & Cuzzone, J. K. 2020: Maximum southwest Greenland Ice Sheet recession in the early Holocene. *Geophysical Research Letters 47*, e2019GL083164. https://doi.org/10.1029/2019GL083164.

Levy, L. B., Kelly, M. A., Lowell, T. V., Hall, B. L., Hempel, L. A., Honsaker, W. M., Lusas, A. R., Howey, J. A. & Axford, Y. L. 2014: Holocene fluctuations of Bregne ice cap, Scoresby Sund, east Greenland: a proxy for climate along the Greenland Ice Sheet margin. *Quaternary Science Reviews 92*, 357–368. https://doi.org/10.1016/j.quascirev.2013.06.024.

Li, Y. 2018: Determining topographic shielding from digital elevation models for cosmogenic nuclide analysis: a GIS model for discrete sample sites. *Journal of Mountain Science 15*, 939–947. https://doi.org/10.1007/s11629-018-4895-4.

Li, Y. 2023: PalaeoIce: an automated method to reconstruct palaeoglaciers using geomorphic evidence and digital elevation models. *Geomorphology 421*, 108523. https://doi.org/10.1016/j.geomorph.2022.108523.

Licciardi, J. M., Denoncourt, C. L. & Finkel, R. C. 2008: Cosmogenic ^{36}Cl production rates from Ca spallation in Iceland. *Earth and Planetary Science Letters 267*, 365–377. https://doi.org/10.1016/j.epsl.2007.11.036.

Lifton, N., Sato, T. & Dunai, T. J. 2014: Scaling in situ cosmogenic nuclide production rates using analytical approximations to atmospheric cosmic-ray fluxes. *Earth and Planetary Science Letters 386*, 149–160. https://doi.org/10.1016/j.epsl.2013.10.052.

Maizels, J. K. & Dugmore, A. J. 1985: Lichenometric dating and tephrochronology of sandur deposits, Sólheimajökull area, southern Iceland. *Jökull 35*, 69–78.

Marrero, S. M., Phillips, F. M., Caffee, M. W. & Gosse, J. C. 2016: CRONUS – earth cosmogenic 36Cl calibration. *Quaternary Geochronology 31*, 199–219. https://doi.org/10.1016/j.quageo.2015.10.002.

Martin, L., Blard, P.-H., Balco, G., Lave, J., Delunel, R., Lifton, N. & Laurent, V. 2017: The CREp program and the ICE-D production rate calibration database: a fully parameterizable and updated online tool to compute cosmic-ray exposure ages. *Quaternary Geochronology 38*, 25–49. https://doi.org/10.1016/j.quageo.2016.11.006.

McCarthy, D. P. & Zaniewski, K. 2001: Digital analysis of lichen cover: a technique for use in lichenometry and licnenology. *Arctic, Antarctic, and Alpine Research 33*, 107–113. https://doi.org/10.1080/15230430.2001.12003411.

Meier, M. F. & Post, A. S. 1962: Recent variations in mass net budgets of glaciers in western North America. *International Association of Scientific Hydrology. Publication 58*, 63–77.

Merchel, S., Bremser, W., Alfimov, V., Arnold, M., Aumaître, G., Benedetti, L., Bourlès, D. L., Caffee, M., Fifield, L. K., Finkel, R. C., Freeman, S. P. H. T., Martschini, M., Matsushi, Y., Rood, D. H., Sasa, K., Steier, P., Takahashi, T., Tamari, M., Tims, S. G., Tosaki, Y., Wilcken, K. M. & Xu, S. 2011: Ultra-trace analysis of ^{36}Cl by accelerator mass spectrometry: an interlaboratory study. *Analytical and Bioanalytical Chemistry 400*, 3125–3132. https://doi.org/10.1007/s00216-011-4979-2.

Moore, A. K. & Granger, D. E. 2019: Calibration of the production rate of cosmogenic 36Cl from Fe. *Quaternary Geochronology 51*, 87–98. https://doi.org/10.1016/j.quageo.2019.02.002.

Nesje, A. & Matthews, J. A. 2024: Holocene glacial landscapes of the Scandinavian Peninsula. *In* Palacios, D., Hughes, P., Jomelli, V. & Tanarro, L. M. (eds.): *European Glacial Landscapes*, 245–274. Elsevier, Amsterdam. https://doi.org/10.1016/B978-0-323-99712-6.00020-9.

NorÞdahl, H. & Einarsson, T. 2001: Concurrent changes of relative sea-level and glacier extent at the Weichselian – Holocene boundary in BerufjörÞur, Eastern Iceland. *Quaternary Science Reviews 20*, 1607–1622. https://doi.org/10.1016/S0277-3791(01)00006-3.

NorÞdahl, H. & Pétursson, H. G. 2005: Relative sea level changes in Iceland. New aspects of the Weichselian deglaciation of Iceland. *In* Caseldine, C., Russel, A., HarÞardóttir, J. & Knudsen, Ó. (eds.): *Iceland – Modern Processes and Past Environments*, 25–78. Elsevier, Amsterdam. https://doi.org/10.1016/S1571-0866(05)80005-3.

NorÞdahl, H., Ingólfsson, Ó., Péturssonn, H. G. & Hallsdóttir, M. 2008: Late Weichselian and Holocene environmental history of Iceland. *Jökull 58*, 343–364. https://doi.org/10.33799/jokull2008.58.343.

Óladóttir, B. A., Thordarson, T., Geirsdóttir, Á., Jóhannsdóttir, G. E. & Mangerud, J. 2020: The Saksunarvatn Ash and the G10ka series tephra. Review and current state of knowledge. *Quaternary Geochronology 56*, 101041. https://doi.org/10.1016/j.quageo.2019.101041.

Osborn, G., McCarthy, D., LaBrie, A. & Burke, R. 2015: Lichenometric dating: science or pseudo-science? *Quaternary Research 83*, 1–12. https://doi.org/10.1016/j.yqres.2014.09.006.

Palacios, D., Gómez-Ortiz, A., Alcalá-Reygosa, J., Andrés, N., Oliva, M., Tanarro, L. M., Salvador-Franch, F., Schimmelpfennig, I., Fernández-Fernández, J. M., Léanni, L. & Aster Team 2019: The challenging application of cosmogenic dating methods in residual glacial landforms: the case of Sierra Nevada (Spain). *Geomorphology 325*, 103–118. https://doi.org/10.1016/j.geomorph.2018.10.006.

Palacios, D., Rodríguez-Mena, M., Fernández-Fernández, J. M., Schimmelpfennig, I., Tanarro, L. M., Zamorano, J. J., Andrés, N., Úbeda, J., Sæmundsson, Þ., Brynjólfsson, S., Oliva, M. & ASTER Team 2021: Reversible glacial-periglacial transition in response to climate changes and paraglacial dynamics: a case study from HéÞinsdalsjökull (northern Iceland). *Geomorphology 388*, 107787. https://doi.org/10.1016/j.geomorph.2021.107787.

Paterson, W. S. B. 1994: *Physics of Glaciers*. 496 pp. Butterworth-Heinemann, Oxford.

Paul, F., Huggel, C. & Kääb, A. 2004: Combining satellite multispectral image data and a digital elevation model for mapping debris-covered glaciers. *Remote Sensing of Environment 89*, 510–518. https://doi.org/10.1016/j.rse.2003.11.007.

Pedersen, R. A. & Christensen, J. H. 2019: Attributing Greenland warming patterns to regional Arctic sea ice loss. *Geophysical*

Research Letters 46, 10495–10503. https://doi.org/10.1029/2019GL083828.
Pellitero, R., Rea, B. R., Spagnolo, M., Bakke, J., Hughes, P., Ivy-Ochs, S., Lukas, S. & Ribolini, A. 2015: A GIS tool for automatic calculation of glacier equilibrium-line altitudes. *Computers & Geosciences 82*, 55–62. https://doi.org/10.1016/j.cageo.2015.05.005.
Pellitero, R., Rea, B. R., Spagnolo, M., Bakke, J., Ivy-Ochs, S., Frew, C. R., Hughes, P., Ribolini, A., Lukas, S. & Renssen, H. 2016: GlaRe, a GIS tool to reconstruct the 3D surface of palaeoglaciers. *Computers and Geosciences 94*, 77–85. https://doi.org/10.1016/j.cageo.2016.06.008.
Pétursson, H. G., Norþdahl, H. & Ingólfsson, Ó. 2015: Late Weichselian history of relative sea level changes in Iceland during a collapse and subsequent retreat of marine based ice sheet. *Cuadernos de Investigación Geográfica 41*, 261–277. https://doi.org/10.18172/cig.2741.
Porter, S. C. 2000: Snowline depression in the tropics during the Last Glaciation. *Quaternary Science Reviews 20*, 1067–1091. https://doi.org/10.1016/S0277-3791(00)00178-5.
Porter, C., Howat, I., Noh, M. J., Husby, E., Khuvis, S., Danish, E., Tomko, K., Gardiner, J., Negrete, A., Yadav, B., Klassen, J., Kelleher, C., Cloutier, M., Bakker, J., Enos, J., Arnold, G., Bauer, G. & Morin, P. 2022: *ArcticDEM – Strips, Version 4.1*. Harvard Dataverse, V1. https://doi.org/10.7910/DVN/C98DVS.
Porter, C., Howat, I., Noh, M. J., Husby, E., Khuvis, S., Danish, E., Tomko, K., Gardiner, J., Negrete, A., Yadav, B., Klassen, J., Kelleher, C., Cloutier, M., Bakker, J., Enos, J., Arnold, G., Bauer, G. & Morin, P. 2023: *ArcticDEM – Mosaics, Version 4.1*. Harvard Dataverse, V1. https://doi.org/10.7910/DVN/3VDC4W.
Principato, S. M. 2008: Geomorphic evidence for Holocene glacial advances and sea level fluctuations on eastern Vestfirþir, northwest Iceland. *Boreas 37*, 132–145. https://doi.org/10.1111/j.1502-3885.2007.00003.x.
Putkonen, J., Connolly, J. & Orloff, T. 2008: Landscape evolution degrades the geologic signature of past glaciations. *Geomorphology 97*, 208–217. https://doi.org/10.1016/j.geomorph.2007.02.043.
Putkonen, J. & Swanson, T. 2003: Accuracy of cosmogenic ages for moraines. *Quaternary Research 59*, 255–261. https://doi.org/10.1016/S0033-5894(03)00006-1.
Rasmussen, S. O., Bigler, M., Blockley, S. P., Blunier, T., Buchardt, S. L., Clausen, H. B., Cvijanovic, I., Dahl-Jensen, D., Johnsen, S. J., Fischer, H., Gkinis, V., Guillevic, M., Hoek, W. Z., Lowe, J. J., Pedro, J. B., Popp, T., Seierstad, I. K., Steffensen, J. P., Svensson, A. M., Vallelonga, P., Vinther, B. M., Walker, M. J. C., Wheatley, J. J. & Winstrup, M. 2014: A stratigraphic framework for abrupt climatic changes during the Last Glacial period based on three synchronized Greenland ice-core records: refining and extending the INTIMATE event stratigraphy. *Quaternary Science Reviews 106*, 14–28. https://doi.org/10.1016/j.quascirev.2014.09.007.
Rasmussen, S. O., Vinther, B. M., Clausen, H. B. & Andersen, K. K. 2007: Early Holocene climate oscillations recorded in three Greenland ice cores. *Quaternary Science Reviews 26*, 1907–1914. https://doi.org/10.1016/j.quascirev.2007.06.015.
Rist, S. 1974: Jöklabreytingar 1931/64, 1964/73, og 1973/74. *Jökull 24*, 77–82.
Sæmundsson, K., Kristjansson, L., McDougall, I. & Watkins, N. D. 1980: K-Ar dating, geological and paleomagnetic study of a 5-km lava succession in northern Iceland. *Journal of Geophysical Research. Solid Earth 85*, 3628–3646. https://doi.org/10.1029/JB085iB07p03628.
Sancho, L. G., Palacios, D., Green, T. A., Vivas, M. & Pintado, A. 2011: Extreme high lichen growth rates detected in recently deglaciated areas in Tierra del Fuego. *Polar Biology 34*, 813–822. https://doi.org/10.1007/s00300-010-0935-4.
Sancho, L. G., Pintado, A., Navarro, F., Ramos, M., De Pablo, M. A., Blanquer, J. M., Raggio, J., Valladares, F. & Green, T. G. A. 2017: Recent warming and cooling in the Antarctic peninsula region has rapid and large effects on lichen vegetation. *Scientific Reports 7*, 5689. https://doi.org/10.1038/s41598-017-05989-4.
Schimmelpfennig, I., Benedetti, L., Garreta, V., Pik, R., Blard, P. H., Burnard, P., Bourlès, D., Finkel, R., Ammon, K. & Dunai, T. 2011: Calibration of cosmogenic ^{36}Cl production rates from Ca and K spallation in lava flows from Mt. Etna (38° N, Italy) and Payun Matru (36° S, Argentina). *Geochimica et Cosmochimica Acta 75*, 2611–2632. https://doi.org/10.1016/j.gca.2011.02.013.
Schimmelpfennig, I., Schaefer, J. M., Putnam, A. E., Koffman, T., Benedetti, L., Ivy-Ochs, S., Team, A. & Schlüchter, C. 2014: ^{36}Cl production rate from K-spallation in the European Alps (Chironico landslide, Switzerland). *Journal of Quaternary Science 29*, 407–413. https://doi.org/10.1002/jqs.2720.
Schimmelpfennig, I., Tesson, J., Blard, P. H., Benedetti, L., Zakari, M. & Balco, G. 2019: *The CREp Chlorine-36 Exposure Age and Depth Profile Calculator*. Goldschmidt, Spain, Barcelona. https://goldschmidtabstracts.info/2019/2996.pdf.
Schweinsberg, A. D., Briner, J. P., Licciardi, J. M., Bennike, O., Lifton, N. A., Graham, B. L., Young, N. E., Schaefer, J. M. & Zimmerman, S. H. 2019: Multiple independent records of local glacier variability on Nuussuaq, West Greenland, during the Holocene. *Quaternary Science Reviews 215*, 253–271. https://doi.org/10.1016/j.quascirev.2019.05.007.
Sigfúsdóttir, T. & Benediktsson, Í. Ö. 2020: Refining the history of Younger Dryas and Early Holocene glacier oscillations in the Borgarfjörþur region, western Iceland. *Boreas 49*, 296–314. https://doi.org/10.1111/bor.12424.
Sigfúsdóttir, T., Benediktsson, Í. Ö. & Phillips, E. 2018: Active retreat of a Late Weichselian marine-terminating glacier: an example from Melasveit, western Iceland. *Boreas 47*, 813–836. https://doi.org/10.1111/bor.12306.
Solomina, O., Bushueva, I. S. & Glazovsky, A. F. 2024: Holocene glacial landscapes of the Russian Arctic and the Urals. *In* Palacios, D., Hughes, P., Jomelli, V. & Tanarro, L. M. (eds.): *European Glacial Landscapes*, 149–169. Elsevier, Amsterdam. https://doi.org/10.1016/B978-0-323-99712-6.00019-2.
Søndergaard, A. S., Larsen, N. K., Olsen, J., Strunk, A. & Woodroffe, S. 2019: Glacial history of the Greenland Ice Sheet and a local ice cap in Qaanaaq, northwest Greenland. *Journal of Quaternary Science 34*, 536–547. https://doi.org/10.1002/jqs.3139.
Stone, J. O. 2000: Air pressure and cosmogenic isotope production. *Journal of Geophysical Research 105*, 23753–23759. https://doi.org/10.1029/2000JB900181.
Stötter, J. 1991: New observations on the postglacial glacial history of Tröllaskagi, northern Iceland. *In* Maizels, J. K. & Caseldine, C. (eds.): *Environmental Change in Iceland: Past and Present*, 181–192. Springer, Dordrecht. https://doi.org/10.1007/978-94-011-3150-6_12.
Stötter, J., Wastl, M., Caseldine, C. & Häberle, T. 1999: Holocene palaeoclimatic reconstruction in northern Iceland: approaches and results. *Quaternary Science Reviews 18*, 457–474. https://doi.org/10.1016/S0277-3791(98)00029-8.
Striberger, J., Björck, S., Holmgren, S. & Hamerlík, L. 2012: The sediments of Lake Lögurinn – a unique proxy record of Holocene glacial meltwater variability in eastern Iceland. *Quaternary Science Reviews 38*, 76–88. https://doi.org/10.1016/j.quascirev.2012.02.001.
Sutherland, D. G. 1984: Modern glacier characteristics as a basis for inferring former climates with particular reference to the Loch Lomond Stadial. *Quaternary Science Reviews 3*, 291–309. https://doi.org/10.1016/0277-3791(84)90010-6.
Tanarro, L. M., Palacios, D., Fernández-Fernández, J. M., Andrés, N., Oliva, M., Rodríguez-Mena, M., Schimmelpfennig, I., Brynjólfsson, S., Sæmundsson, T., Zamorano, J. J., Úbeda, J. & Aster Team 2021: Origins of the divergent evolution of mountain glaciers during deglaciation: Hofsdalur cirques, Northern Iceland. *Quaternary Science Reviews 273*, 107248. https://doi.org/10.1016/j.quascirev.2021.107248.
Thompson, A. & Jones, A. 1986: Rates and causes of proglacial river terrace formation in southeast Iceland: an application of lichenometric dating techniques. *Boreas 15*, 231–246. https://doi.org/10.1111/j.1502-3885.1986.tb00928.x.
Thorarinsson, S. 1946: Oscillations of the Iceland glaciers in the last 250 years. *Geografiska Annaler 25*, 1–54. https://doi.org/10.1080/20014422.1943.11880716.
Thorarinsson, S. 1949: Some tephrochronological contributions to the volcanology and Glaciology of Iceland. *Geografiska Annaler 31*, 239–256. https://doi.org/10.1080/20014422.1949.11880809.

Uppala, S. M. and 45 others 2005: The ERA-40 re-analysis. *Quarterly Journal of the Royal Meteorological Society 131*, 2961–3012. https://doi.org/10.1256/qj.04.176.

Van der Veen, C. J. 1999: *Fundamentals of Glacier Dynamics*. 462 pp. Balkema, Rotterdam.

Vinther, B. M., Clausen, H. B., Johnsen, S. J., Rasmussen, S. O., Andersen, K. K., Buchart, S. L., Dahl-Jensen, D., Seierstad, I. K., Siggaard-Andersen, M.-L., Steffensen, J. P., Svensson, A., Olsen, J. & Heinemeier, J. 2006: A synchronized dating of three Greenland ice cores throughout the Holocene. *Journal of Geophysical Research 111*, D013102. https://doi.org/10.1029/2005JD006921.

Wastl, M. & Stötter, J. 2005: Holocene glacier history. *In* Caseldine, C., Russell, A., Harðardóttir, J. & Knudsen, Ó. (eds.): *Developments in Quaternary Science 5*, 221–240. Elsevier, Amsterdam. https://doi.org/10.1016/S1571-0866(05)80011-9.

Young, N. E. & Briner, J. P. 2015: Holocene evolution of the western Greenland Ice Sheet: assessing geophysical ice-sheet models with geological reconstructions of ice-margin change. *Quaternary Science Reviews 114*, 1–17. https://doi.org/10.1016/j.quascirev.2015.01.018.

Young, N. E., Briner, J. P., Miller, G. H., Lesnek, A. J., Crump, S. E., Thomas, E. K., Pendleton, S. L., Cuzzone, J., Lamp, J., Zimmerman, S., Caffee, M. & Schaefer, J. M. 2020: Deglaciation of the Greenland and Laurentide ice sheets interrupted by glacier advance during abrupt coolings. *Quaternary Science Reviews 229*, 106091. https://doi.org/10.1016/j.quascirev.2019.106091.